Northern Eurasian rhinocerotines (Mammalia, Perissodactyla) by the Pliocene–Pleistocene transition: phylogeny and historical biogeography

Luca Pandolfi, Antoine Pierre-Olivier, Maia Bukhsianidze, David Lordkipanidze & Lorenzo Rook

View supplementary material

Published online: 29 Nov 2021.

Submit your article to this journal

View related articles

View Crossmark data

Taylor & Francis
Taylor & Francis Group

Check for updates

Northern Eurasian rhinocerotines (Mammalia, Perissodactyla) by the Pliocene–Pleistocene transition: phylogeny and historical biogeography

Luca Pandolfi[a]* (ID), Antoine Pierre-Olivier[b] (ID), Maia Bukhsianidze[c] (ID), David Lordkipanidze[c] (ID) and Lorenzo Rook[a] (ID)

[a]*Dipartimento di Scienze della Terra, Università di Firenze, Via G. La Pira 4, 50121 Firenze, Italy;* [b]*Institut des Sciences de l'Evolution, Université de Montpellier, CNRS, IRD, EPHE, F-34095 Montpellier, France;* [c]*Georgian National Museum, 3, Rustaveli ave., Tbilisi-0105, Georgia*

Pliocene and earliest Pleistocene Northern Eurasian rhinocerotines are poorly documented and understudied in comparison to Pleistocene and Miocene ones. However, they represent a key-group of species for understanding the phylogeny and historical biogeography of their Pleistocene relatives. In the present paper, we revise the abundant material from the late Pliocene locality of Kvabebi, Georgia from a systematic, phylogenetic and palaeobiogeographical perspective. The specimens from Kvabebi are documented by two partially preserved skulls, one mandible and several postcranial remains. Morphological and morphometric comparison with the type material assigned to Pliocene and earliest Pleistocene Northern Eurasian Rhinocerotinae reveal that the specimens from Kvabebi have close affinities with the poorly known *Dicerorhinus miguelcrusafonti* Guérin & Santafé-Llopis, 1978, described from Layna (Spain). The latter species, represented by scanty remains from the Iberian Peninsula, is usually excluded from morphological and morphometrical comparisons and no findings were reported after the 1990s. Pliocene rhinocerotine species have monotonous dental and postcranial morphologies and only a few features allow us to discern the different species. The material from Layna and Kvabebi is somewhat smaller than that of other Pliocene taxa, except for the largest representatives of *Stephanorhinus etruscus* (Falconer, 1868). Accordingly, the earliest specimens assigned to *S. etruscus* on morphometric grounds should be revised in the light of the new data here presented. A cladistic analysis performed on 280 characters and 30 species suggests that the emblematic early Pliocene European species, '*Dihoplus*' *megarhinus* (de Christol, 1834), is sister taxon to the Layna and Kvabebi rhinoceroses. Accordingly, both species are here assigned to a new genus named *Pliorhinus* gen. nov. Although distinct, this clade has close affinities with the paraphyletic genus *Stephanorhinus*, therefore suggesting the co-occurrence of at least two distinct rhinocerotine lineages raised in the late Miocene interval in Northern Eurasia.

http://zoobank.org/urn:lsid:zoobank.org:pub:D3A1AB6D-EFE7-4813-AE74-A27D204A18CA

Keywords: morphology; morphometry; phylogeny; *Pliorhinus* gen. nov.; Eurasia; Pliocene

Introduction

During the last decades, Eurasian fossil Rhinocerotidae were a subject of research for several scholars who proposed different taxonomic combinations and phylogenetic hypotheses (Guérin 1982; Fortelius *et al.* 1993; Cerdeño 1995; Heissig 1996; Antoine *et al.* 2010; Cappellini *et al.* 2019). Among this family, the Pliocene–Pleistocene rhinocerotine species of Eurasia have been the subject of extensive investigation since the eighteenth century, with pioneering studies by eminent palaeontologists such as Cuvier (1822), de Christol (1834) and Falconer (1868). Despite the long history of research on this topic, the group remains poorly understood, and some taxa, in particular the Pliocene species, have been severely under-investigated ever since. The available knowledge on Pliocene rhinocerotines is usually limited to the specimens collected from a few Western European localities

and recently Greece (Guérin & Tsoukala 2013) whilst, elsewhere in Eurasia, Pliocene records are either rare or poorly studied, leaving a gap in the knowledge on the anatomy, phylogenetic relationships, and historical biogeography of rhinocerotines.

Rhinocerotina groups recent rhinos and their kin (Antoine 2002; Antoine *et al.* 2021). It is the only rhinocerotid clade that survived after early Pliocene times, with '*Dihoplus*' *megarhinus* (de Christol 1834), *Stephanorhinus jeanvireti* (Guérin, 1972) and '*Stephanorhinus*' *miguelcrusafonti* (Guérin & Santafé-Llopis, 1978) as conspicuous elements of Northern Eurasian mammalian assemblages described in the last centuries. *Stephanorhinus etruscus* (Falconer, 1868) was also recently recognized from a few late Pliocene European localities (Pandolfi *et al.* 2017) while a new species, '*Dihoplus*' *bethlehemsis*, was described from the latest Pliocene of the Levant (Pandolfi *et al.* 2020). The phylogenetic relationships among these Pliocene taxa as well as their
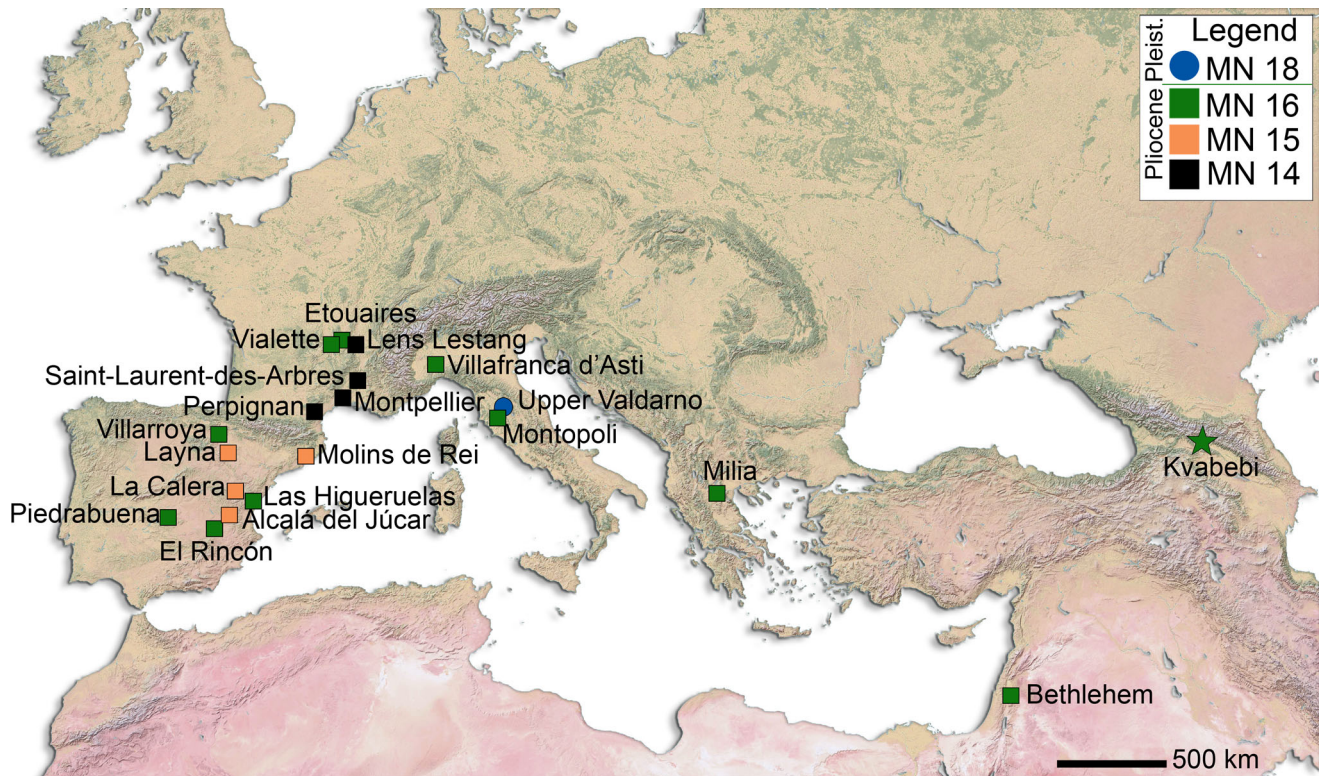

Figure 1. Geographical map showing the position of selected localities discussed in the text. The interactive map with data on species, age and main references is available as Supplemental Fig. S1). The database of Pliocene European localities is reported as in Supplemental Table S1.

diagnostic morphological characters and chronological distribution remain controversial and unclear.

Here we revise the rhinoceros fossil material from the late Pliocene site of Kvabebi (Fig. 1), located in eastern Georgia (Vekua 1972; Agustí *et al.* 2009; Rook *et al.* 2017; Bukhsianidze & Koiava 2018; Lazarev 2020), in order to provide an exhaustive systematic assignment of the collected specimens, which in turn allows us to investigate the phylogenetic relationships and historical biogeography of Pliocene and earliest Pleistocene Eurasian Rhinocerotina.

Kvabebi is located in the Sighnaghi region (eastern Georgia), on the Iori Plateau, which is part of the sedimentary infill of the Kura Basin. Recent field study and surveys allowed a re-evaluation of the geochronological setting of the Kvabebi section (Agustí *et al.* 2009; Bukhsianidze & Koiava 2018; Lazarev 2020) and a revision of the celebrated vertebrate fauna assemblage known since the pivotal study of Abesalom Vekua (Vekua 1972).

Material and methods

Specimens and comparison
The rhinoceros remains collected at Kvabebi are currently housed at the Simon Janashia Museum of

Georgia, Georgian National Museum. The complete list of specimens is reported in Supplemental Table S2.

The morphological and morphometric comparisons are mainly based on direct observations of the Pliocene material housed in several institutions and museums, collected from the type locality or distribution area of the considered species (Table 1). The classification above genus level follows Antoine *et al.* (2010). The dental terminology (Fig. 2) and the morphometric methodology follow Antoine (2002) and Guérin (1980), respectively. The postcranial terminology follows the morphological features as listed and illustrated in Antoine (2002). The studied specimens were measured using a digital calliper. Comparative tables are reported in the Supplemental Tables S3–S16. A number of the Kvabebi specimens were acquired using the structured blue led light 3D Scanner Artec Eva and Artec Space Spider. A selection of downloadable 3D models is available in the Supplemental materials.

Institutional and collection abbreviations
GNM1, Simon Janashia Museum of Georgia, Georgian National Museum, Tbilisi, Georgia; **HNHM**, Hungarian

Table 1. Pliocene–earliest Pleistocene Rhinocerotidae species included in the comparison section.

Species	Locality	Age	Collection	Reference
Rhinoceros megarhinus	Montpellier	Early Pliocene, MN14	NHMUK, MNHN, NMB,	de Christol 1834
Rhinoceros etruscus	Upper Valdarno (various localities)	Early Pleistocene, MNQ18	MGG, MNCN, NHMF (IGF), NMB	Falconer 1868
Dicerorhinus jeanvireti	Vialette	Latest Pliocene, MN16a, *c.* 3.14 Ma	NMB	Guérin 1972
Dicerorhinus miguelcrusafonti	Layna	Middle Pliocene, MN14, *c.* 4Ma	MNCN	Guérin & Santafé-Llopis 1978
'*Dihoplus*' *bethlehemsis*	Bethlehem	Latest Pliocene, MN16a	NHMUK	Pandolfi *et al.* 2020
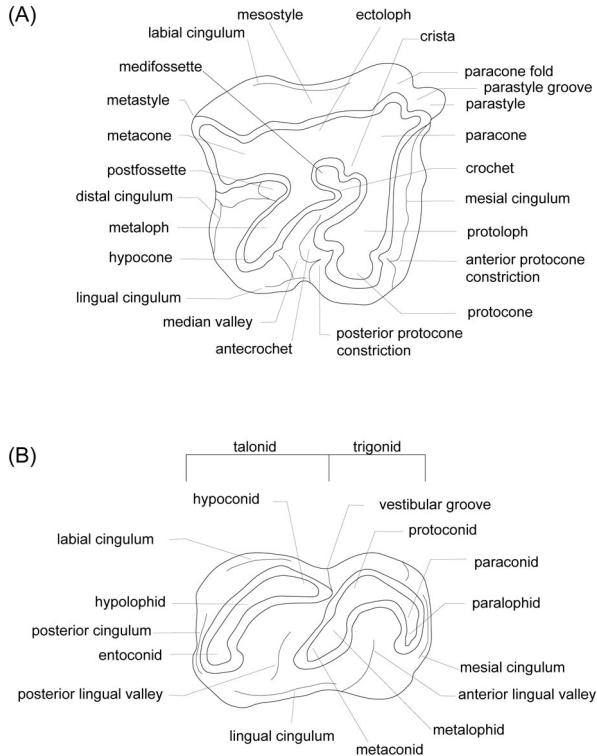
Figure 2. Nomenclature of **A,** upper and **B,** lower teeth used in the text.

Natural History Museum, Budapest, Hungary; **k**, Kvabebi; **IGF**, Museo di Storia Naturale, sezione di Geologia e Paleontologia, Florence, Italy; **IPS**, Provincial Institute of Paleontology (now Institut Català de Paleontologia Miquel Crusafont), Sabadell, Spain; **IVPP**, Institute of Vertebrate Paleontology and Paleoanthropology, Chinese Academy of Sciences, Beijing, China; **MGG**, Museo di Geologia Giovanni Capellini, Bologna, Italy; **MNCN**, Museo Nacional de Ciencias Naturales, Madrid, Spain; **MNHN**, Muséum national d'Histoire naturelle, Paris, France; **NHMUK**, Natural History Museum, London, UK; **NMB**, Naturhistorisches Museum, Basel, Switzerland.

Anatomical abbreviations

dp, lower deciduous; **DP**, upper deciduous; **m**, lower molar; **M**, upper molar; **Mc**, metacarpal; **Mt**, metatarsal; **p**, lower premolar; **P**, upper premolar.

Measurement abbreviations

a, articular surface; **DAP**, anteroposterior diameter; **DAPm**, medial anteroposterior diameter; **D**, distal epiphysis; **DTD**, distal transverse diameter; **DTDa**, distal transverse diameter of the articular surface; **DTP**, transverse diameter of the proximal articular surface; **H**, height; **Hm**, medial height; **L**, length; **Lm**/**LM**, length of the lower/upper molars; **LMax**, maximal length; **Lp**/**LP**, length of the lower/upper premolars; **LP3**–**P4**, length of the upper third and fourth premolars; **Lp3**–**p4**, length of the lower third and fourth premolars; **Ltot**, total length; **max**, maximal; **P**, proximal epiphysis; **S**, shaft (diaphysis); **TD**, transverse diameter; **TDS**, transverse diameter of the diaphysis.

Cladistic analysis

A cladistic analysis is performed in order to investigate the phylogenetic relationships of the Kvabebi rhinoceros. The character matrix includes 280 cranio-mandibular, dental, and postcranial characters, including 278 characters adapted from Antoine *et al.* (2021), plus characters 8 and 13 from Antoine (2002) (Supplemental text S1). The character states were mostly coded through direct observations by LP and POA. With respect to the matrix originally described in Antoine (2002), characters 29, 30, 32, 43, 52, 64, 93, 96, 106, 123, 127, 132, 136, 167 and 195 were not included here as they were primarily relevant for Elasmotheriinae only. Conversely, characters 17 (cranial), 59, 91, 99, 146, 172 (dental), 183, 198, 218, 255, 266 and 270 (postcranial), newly described by Antoine *et al.* (2021), were included as they describe evolutionary patterns among Rhinocerotina. All characters are equally weighted. Most multistate characters were treated as additive, and only six multistate characters were considered as non-

additive (characters 68, 89, 97, 131, 179 and 265). The analysis is performed with PAUP 4.0β10 (Swofford 2001), Heuristic search, TBR and 1000 replications with additional random sequence, gaps treated as missing. Twenty-nine terminal taxa were included in this analysis. The outgroup is represented by four taxa: the Brazilian tapir (*Tapirus terrestris*), the early rhinocerotoid *Hyrachyus eximius*, and the early-diverging Rhinocerotidae *Trigonias osborni* and *Ronzotherium filholi*. The ingroup includes a comprehensive sample of Rhinocerotina and selected representatives of other suprageneric clades of interest among Rhinocerotidae (i.e. Elasmotheriinae, Aceratheriini and Teleoceratina). The data matrix is provided in Supplemental text S2.

Systematic palaeontology

Order **Perissodactyla** Owen, 1848
Family **Rhinocerotidae** Gray, 1821
Subfamily **Rhinocerotinae** Gray, 1821
Tribe **Rhinocerotini** Gray, 1821
Subtribe **Rhinocerotina** Gray, 1821
Genus ***Pliorhinus*** gen. nov.

Type species. *Pliorhinus megarhinus* (de Christol, 1834) comb. nov.

Emended diagnosis of the type species. Relatively large-sized two-horned rhinoceros with a flat dorsal profile of the skull, a convex cross section of the processus postglenoidalis, a labial cingulum usually absent on the upper premolars and molars, a crochet usually present on P2–P4, a separate protocone and hypocone on P2, a lingual bridge on P3 and P4, an absence of antecrochet on P4, a crista usually present on the upper molars, a medifossette usually absent on the upper molars, an external groove vanishing before the neck on the lower cheek teeth, a lingual cingulum usually absent on the lower molars, an ectolophid fold present on d2 and d3, an anterodistal groove present on the tibia, an unfused tibia and fibula, a slender tuber calcanei, and a salient insertion of the m. fibularis longus on the calcaneus.

Included species. *Pliorhinus miguelcrusafonti* (Guérin & Santafé-Lopis, 1978) comb. nov.

Derivation of name. From the Greek word pleíōn (more), as used in the name Pliocene, and the suffix -rhinus (nose), often used for depicting rhinocerotid taxa.

Diagnosis. Medium- to large-sized two-horned Rhinocerotina with foramen infraorbitalis and nasal notch located above the molars, high zygomatic arch, occipital face backward inclined, developed nuchal tubercle, sub-triangular foramen magnum, P1 usually absent in adults, transverse metaloph on P2, protoloph always interrupted on P2, constriction of the protocone usually absent on P3 and P4, crista always present on P3, posterior part of the ectoloph concave on M1 and M2, constriction of the protocone always absent on M3, angular trigonid on the lower teeth, obtuse or right dihedron trigonid on the lower teeth, smooth anterior side of the semilunate, mediolaterally symmetric distal facet for the semilunar on the pyramidal, and curved magnum-facet on McII.

Pliorhinus differs from *Dicerorhinus* in having the foramen infraorbitalis above the molars, the nasal notch above P1–P3, a short contact between nasal and lachrymal bones, the anterior border of the orbit above the M2–M3, a high zygomatic arch, a flat area between the temporal and the nuchal crests on the squamosal, a totally closed external auditory pseudomeatus, a nearly vertical posterior margin of the pterygoid, anteriorly fused nasal bones, a ratio between the zygomatic width and the frontal width more than 1.5, a straight transverse profile of the articular tubercle on the squamosal, a little-developed processus post-tympanicus, the foramen mental at the level of p2–p4, a backward-inclined mandibular ramus, a well-developed processus coronoideus, the first upper and lower incisors absent, an incisor-like shape of the second lower incisor, a metaloph constriction on the upper premolars, an antecrochet usually absent on P2 and P3, the P1 usually absent, a transverse metaloph on P2, a protocone less strong than hypocone of P2, a crista always present on P3, an antecrochet usually absent on the upper molars, a crochet always present on the upper molars, a strong paracone fold on M1 and M2, a long metaloph on M1 and M2, a concave posterior part of the ectoloph on M1 and M2, a posterior cingulum low and interrupted on M1 and M2, an isolated hypocone on M1, an angular trigonid on the lower teeth, trigonid with acute dihedron on the lower teeth, 'V'-shaped lingual valleys on the lower premolars, d1/p1 always absent, an isolated paralophid on p2, a posterior valley on d2 usually open, a lingual groove on the entoconid always absent on d3, straight axis-facets on the atlas, a very elongated scapula, an oval glenoid fossa on the scapula, a low oleocranic fossa on the humerus, the proximal ulna-facets always separated on the radius, a deep and wide gutter for the extensor carpi muscles on the radius, an open angle between the diaphysis and the oleocranon on the ulna, a rounded distal border of the anterior side of the semilunar, a symmetric distal facet for the semilunate on the pyramidal, an elliptic distal side on the pyramidal, the absence of the indentation on the medial side of the magnum, a curved magnum-

facet on McII, a sub-triangular acetabulum on the coxal bone, a high and narrow fovea capitis on the femur, a very developed third trochanter, a curved proximal border of the patellar trochlea, a mediodistal gutter always present on the tibia, a low and rounded posterior apophysis on the tibia, a high collum tali on the astragalus, a very oblique orientation between the trochlea and the distal articulation, the calcaneus-facets 2 and 3 always fused, an oval proximal side of the cuboid, a sigmoid proximal border of the anterior side on MtIII, the cuboid-facet absent on MtIII, and low and smooth intermediate reliefs on the metapodials.

Pliorhinus differs from *Dihoplus* species in having a foramen infraorbitalis above the molars, a nasal notch above P4–M1, a short contact between nasal and lacrymal bones, a totally closed external auditory pseudomeatus, a backward inclined occipital side, a developed nuchal tubercle, a tooth row placed in the anterior half of the skull, a nearly vertical posterior border of the pterygoid, a ratio between the zygomatic width and the frontal width equals or is more than 1.5, a sub-triangular foramen magnum, the absence of a median ridge on the occipital condyle, a straight base of the corpus mandibulae, a crista always present on P3, a metacone and hypocone joined on P4, a concave posterior part of the ectoloph on M1 and M2, a constriction of the protocone always absent on M3, an acute trigonid on the lower teeth, a mesostyle present on D3 and D4, the absence of entoconid constriction on the lower deciduous teeth, a double paralophid on d3, a straight anterior border of the proximal articulation on the radius, a shallow insertion for the m. biceps brachii on the radius, a curved posterior tuberosity on the magnum, a pyramidal and McV facets always separated on the unciform, a posterior McIII-facet always absent on McII, a mediodistal gutter always present on the tibia, a low and rounded posterior apophysis on the tibia, a high collum tali on the astragalus, a fibula-facet always absent on the calcaneus, a tibia-facet always absent on the calcaneus, a lozenge-shaped cross-section of the navicular in proximal view, the absence of a distal widening of the diaphysis on MtIII, the absence of the cuboid-facet on MtIII, and a symmetrical insertion for MtIII nearly anteriorly placed on the first phalanx.

Pliorhinus differs from *Stephanorhinus* species in having the foramen infraorbitalis above the molars, a low base of the processus zygomaticus maxillari, a backward inclined occipital face, a developed nuchal tubercle, a foramen mandibulare above the tooth-row, a wrinkled enamel, a wide postfossette on the upper premolars, a lingual cingulum usually absent on the upper premolars, protocone and hypocone forming a lingual bridge on P2, a transverse metaloph on P2, an interrupted protoloph on P2, a medifossette absent on P3 and P4, a protocone usually constricted on P3 and P4, a protocone always constricted on M1 and M2, a strong paracone fold on M1 and M2, an angular trigonid on the lower teeth, an oblique hypolophid on the lower molars, a mediolaterally symmetric distal facet for semilunate on the pyramidal, a curved magnum-facet on McII, a trapezium-facet usually present on McII, and in lacking the tibia-facet on the calcaneus.

Pliorhinus miguelcrusafonti (Guérin & Santafé-Lopis, 1978) comb. nov.

(Figs 3–11)

1972 *Dicerorhinus megarhinus* (Christol); Vekua: 161.
1987 *Dicerorhinus vekuai* Tsiskarishvili: 81–91, tables 10–13, pls 26, 27.
2008 *Dicerorhinus megarhinus* Vekua & Lordkipanidze: 151.
2009 *Stephanorhinus megarhinus* Agustí *et al.*: 3277.
2017 *Stephanorhinus megarhinus* (de Christol, 1834); Rook *et al.*: 1259.
2018 *Stephanorhinus megarhinus* (de Christol, 1834); Bukhsianidze & Koiava: 453.

Holotype. Fragment of hemi-mandible IPS La 15632 collected from the Pliocene locality of Layna, described and figured by Guérin & Santafé-Llopis (1978, pl. 2, 3A).

Emended diagnosis. Representative of *Pliorhinus* with a low base of the processus zygomaticus maxillari, a foramen mandibulare above teeth-neck level, a wrinkled aspect of the enamel, a multiple crochet on the premolars, a continuous or usually reduced lingual cingulum on the premolars, a wide postfossette on the premolars, no medifossette on P3 and P4, a constriction of the protocone usually present on P3, P4 and always present on M1 and M2, a posterior valley usually open on p2, secondary folds on DP2, not visible trapezium-facet on McII. From a metric perspective, specimens of *P. miguelcrusafonti* are somewhat smaller than those of *P. megarhinus* and of *Stephanorhinus jeanvireti* and are close to those of the largest individuals of *S. etruscus*.

Pliorhinus miguelcrusafonti differs from *P. megarhinus* in having a low base of the processus zygomaticus maxillari, a concave dorsal profile of the skull, a right dihedron processus postglenoidalis, a foramen mandibulare above teeth-neck level, a wrinkled aspect of the enamel, a labial cingulum absent on the upper molars, a crochet always present on the upper premolars, a lingual cingulum usually absent on the upper premolars, a wide postfossette on the upper premolars, separated protocone and hypocone on the upper premolars, an

antecrochet always absent on P4, an external groove reaching the neck on the lower teeth, a posterior valley usually opened on p2, a lingual cingulum always absent on the lower molars, secondary folds present on DP2, a diabolo-shaped distal articulation on the humerus, a trapezium-facet usually present on McII, an anterodistal groove absent on the tibia, a contact between tibia and fibula, a tibia-facet absent on the calcaneus, a massive tuber calcanei, an invisible insertion of the m. fibularis longus on the calcaneus, a separated posteromedial facet from the proximal facet on the cuboid.

Referred material. GNM1 29-2013/300 (K744), neurocranial portion of skull; GNM1 29-2013/925, a crushed skull bearing the right P2–M3; GNM1 29-2013/925, a horizontal ramus of the mandible bearing p3–m3; GNM1 29-2013/278, a fragment of left mandible bearing p3 and p4; GNM1 29-2013/288 (K86), a left M3; GNM1 29-2013/290 (K85), a right P4; GNM1 29-2013/286 (K80), a right D3; GNM1 29-2013/285 (K75), a right D4; GNM1 29-2013/287 (K79), a right D4; GNM1 29-2013/284 (K88-K89), a right M2–M3; GNM1 29-2013/282 (K905), a right d3; GNM1 29-2013/279 (K82), a right m3; GNM1 29-2013/270 (K760), a proximal epiphysis of a left radius with a fragment of ulna; GNM1 29-2013/271 (K355 or K399), a fragment of right distal epiphysis of radius and ulna; GNM1 29-2013/273 (K753), an almost complete left ulna; GNM1 29-2013/274 (K505), a distal epiphysis of a left tibia; GNM1 29-2013/275 (K71), a proximal epiphysis of a right Mt3; GNM1 29-2013/276, a proximal epiphysis of a right radius; GNM1 29-2013/277 (K65), a damaged first lateral phalanx; GNM1 29-2013/292 (K492), a mesiolingual fragment of a right upper premolar; GNM1 29-2013/293 (K81), a fragment of protocone of a left upper deciduous; GNM1 29-2013/294 (K493), a fragment of an upper premolar; GNM1 29-2013/295 (K500), a lingual fragment of a lower molar; GNM1 29-2013/296 (K496), a fragment of an upper tooth; GNM1 29-2013/297 (K497), a vestibular fragment of right upper molar; GNM1 29-2013/302 (K767), a right humerus; GNM1 29-2013/342 (K61), a left scaphoid; GNM1 29-2013/343 (K70), a left unciform; GNM1 29-2013/344 (K53), a left unciform; GNM1 29-2013/345 (K74), a fragment of left magnum; GNM1 29-2013/347 (K63), a fragment of magnum; GNM1 29-2013/348 (K908), a right semilunar; GNM1 29-2013/349 (K67), a left pyramidal; GNM1 29-2013/350 (K60), a left trapezoid; GNM1 29-2013/496 (K426), a lingual fragment of a left (second?) upper deciduous; GNM1 29-2013/537 (K3047), a proximal fragment of a right femur; GNM1 29-2013/539, a distal fragment of a right humerus; GNM1 29-2013/541 (K4240), a fragment of diaphysis of radius; GNM1 29-2013/542 (K3068), a fragment of long bone; GNM1 29-2013/631 (K3042) a proximal fragment of a left calcaneus; GNM1 29-2013/720 (K4467), a fragment of humerus; GNM1 29-2013/752 (K533), a right tibia; GNM1 29-2013/756 (K69), a left calcaneus; GNM1 29-2013/758 (K72), a right Mc3; GNM1 29-2013/759 (K64), a left Mc2; GNM1 29-2013/760, a fragment of long bone; GNM1 29-2013/761 (K901), a right astragalus; GNM1 29-2013/766 (K3106), a fragment of diaphysis of a right humerus; GNM1 29-2013/929 (K759), a proximal fragment of a left ulna; GNM1 29-2013/930 (K737), a fragment of femur; GNM1 29-2013/931, a proximal fragment of humerus; GNM1 29-2013/933 (K66), a distal fragment of a left Mt3; GNM1 29-2013/934 (K73), a proximal fragment of a right Mt4; GNM1 29-2013/281 (K84), a worn left lower molar. Further, the following specimens were reported by Vekua (1972) but they are not present in the collection: K525, a fragment of fibula (Vekua 1972, pp. 161, 173); K495, a P2 (Vekua 1972, pp. 161, 164); K77, a left D3 (Vekua 1972, pp. 161–163, pl. XXIII, fig. 2); K78, a left D2 (Vekua 1972, pp. 161–163, pl. XXIII, fig. 2); K78, a left D4 (Vekua 1972, pp. 161–163, pl. XXIII, fig. 2); K62, a trapezium (Vekua 1972, p. 169); K902, a navicular (Vekua 1972, pp. 161, 174).

Description
Skull. The dorsal profile of the skull is very concave in its preserved portion, and the frontal-parietal crests are not evident (Fig. 3B). In lateral view, the neurocranial portion GNM1 29-2013/300 (K744) is massive (Fig. 3A). The external auditory pseudo-meatus is ventrally closed, whilst the area between the temporal and nuchal crest is depressed and filled by hard sediment. The occipital face is slightly sloped backward and upward (Fig. 3B), the nuchal crest extends over the occipital condyles and the nuchal tubercle is developed. The foramen sphenorbitale and foramen rotundum are fused, the postorbital process is present, and the zygomatic arch is relatively low. In dorsal view, the rugosity on the frontal bones is partially preserved (suggesting the presence of a median frontal horn), the post-orbital constriction is relatively narrow, the frontal-parietal crests are distant and faint, and the posterior border of the nuchal crest is slightly concave. In posterior view, the occipital face is rectangular and relatively wide; the dorsal profile of the nuchal crest is slightly concave, the foramen magnum is sub-triangular and lacks the dorsal incision. In basal view (Fig. 3C), the specimen is poorly preserved; the palatine spine and the vomer are not visible, the pterygoids are lacking, whereas the lacerate, oval and spinous foramina are not visible, due to the bad state of preservation (encrusted in the sediment).
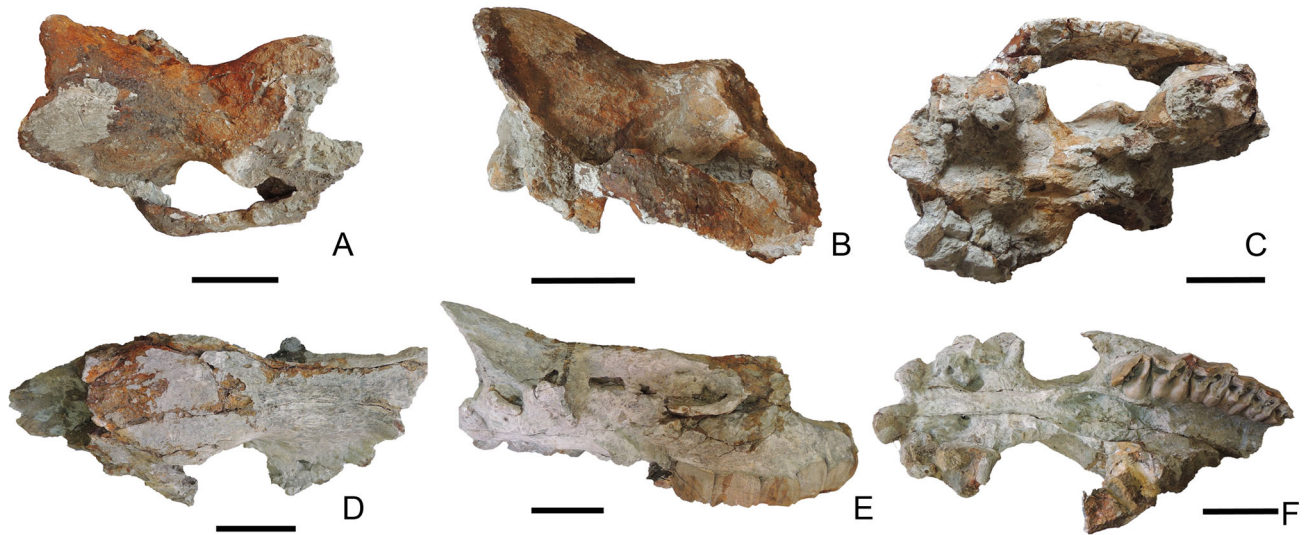
Figure 3. *Pliorhinus miguelcrusafonti* comb. nov. remains from Kvabebi. GNM1 29-2013/300 (K744), neurocranial portion of skull in **A,** dorsal; **B,** lateral; **C,** basal views. GNM1 29-2013/925 DN-229, a crushed skull bearing the right P2–M3 in **D,** dorsal; **E,** lateral; **F,** basal views. Scale bars equal 10 cm.

The right processus postglenoidalis is partially preserved and it appears well developed. The basilar process is poorly preserved, and the presence of a sagittal crest cannot be detected, as well as the position of the foramen nervi hypoglossi.

The skull GNM1 29-2013/925 is partially crushed and lacks the nasal bones and the zygomatic arches (Fig. 3D). In lateral view (Fig. 3E), the dorsal profile is concave (even if deformed), the foramen infraorbitalis is placed above M1, the posterior border of the nasal notch is placed above the anterior third of M1, the anterior border of the orbit is found at the level of M2. The external auditory pseudomeatus is ventrally closed, the occipital face is rather sloped forward, and the nuchal crest extends posteriorly over the occipital condyles. In dorsal view, the frontal bones show an insertion for the median horn; the post-orbital constriction is narrow, whereas the frontal-parietal crests are distant and smooth, and the posterior border of the nuchal crest was most likely concave. In occipital view, the skull is quite deformed, the left-dorsal side is damaged, but some morphological characters can be detected: the dorsal profile of the nuchal crest would be concave, and the occipital face seems to have a low rectangular shape; the foramen magnum is sub-triangular and it lacks the dorsal incision. In basal view (Fig. 3F), the choanae are filled by an encrusted sediment, the lacerate foramen is sub-circular, the intercondyloid fossa is relatively wide and the section of the processus post-glenoidalis is elliptical, even if it is laterally compressed.

The premaxillae are not preserved on the skull GNM1 29-2013/925, so the presence of any elements of the anterior dentition (C and I1-3) cannot be tested. In contrast, this specimen preserves the right maxilla with P2–M3 (Fig. 4A). The premolar series is very long (LP3-P4/LM1-M3 = 0.59). There is coronary cement by places. Enamel has a wrinkled aspect. Crowns are low. The roots of cheek teeth are joined.

The P2 displays a rather convex ectoloph profile with a weak paracone fold, and an elongated parastyle. The mesial side of the tooth does not display a contact facet for a DP1/P1. The protocone is isolated, the mesial cingulum is present, and protocone and hypocone are lingually joined at their bases. A faint crista is present; the crochet is multiple. The metaloph is transversely oriented and partly disconnected from the ectoloph (isolated protocone). The protocone is less developed than the hypocone in lingual view. The postfossette is posteriorly delimited by a complete cingulum and wide, in relation to the transverse orientation of the metaloph.

The P3 has a relatively flat ectoloph profile with a marked paracone fold and an elongated parastyle. The mesial cingulum is present, the lingual cingulum is short and present only at the entrance of the median valley. The protoloph is joined with the ectoloph and protoloph and metaloph are oblique. The metaloph is also 'S'-shaped and the hypocone is slightly constricted. The crista is present, and the crochet is multiple. The postfossette is wide and posteriorly delimited by a cingulum.

The morphology of P4 is similar to that of P3.

The M1 has a concave posterior part of the ectoloph, and a strong paracone fold. The mesostyle is absent,
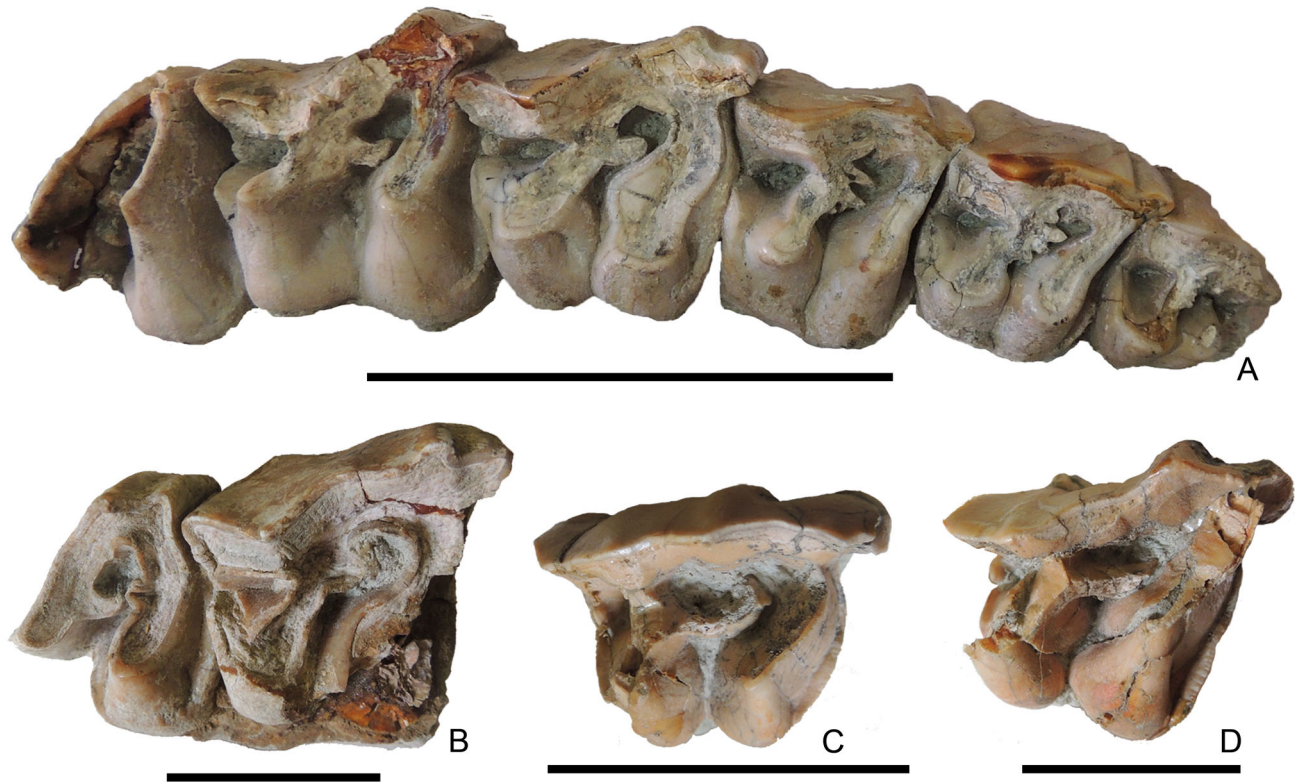
Figure 4. *Pliorhinus miguelcrusafonti* comb. nov. remains from Kvabebi. GNM1 29-2013/925 DN-229, right P2-M3 row in **A,** occlusal view; GNM1 29-2013/284 (K88-K89), right M2-M3 series in **B,** occlusal view; GNM1 29-2013/286 (K80), right D3 in **C,** occlusal view; GNM1 29-2013/285 (K75), right D4 in **D,** occlusal view. Scale bars equal 10 cm for A, and 5 cm for B–D.

and the postfossette is posteriorly delimited by a cingulum. The protoloph is relatively wide, and the protocone is constricted on the distal side. The mesial cingulum is present. The crochet is single, the metaloph is oblique and the hypocone has an incision on its mesial side.

The posterior part of the ectoloph in M2 is more concave than in M1. The crista on M2 is faint, and the crochet is simple. The metaloph is more oblique than the protoloph. The mesial cingulum is present. The protocone is slightly constricted on its distal side and the hypocone has an incision on the mesial side.

The M3 is triangular in occlusal view and it has a quite flat ectoloph profile with a weak paracone fold. The mesial cingulum is present, and the crochet is multiple.

Mandible. The horizontal ramus of the mandible GNM1 29-2013/925 (Fig. 5A–C) is relatively low, and there is only one mental foramen, located below the p2. The vertical ramus is up- and backward inclined, the angulus is rounded and the angular process is weakly developed (no vascular incisure). The mandibular foramen, in lingual view, is placed above the base of the toothrow.

All the lower teeth lack the lingual and labial cingula and display a faint mesial cingulum. The trigonid is rather flat on the labial side in occlusal view. The trigonid is particularly developed on p3, with right angles in occlusal view (forming a characteristic squared-'U' shape). The labial groove is acute, well-marked and deep, and it reaches the base of the crown. The lingual valleys have a narrow 'V'-shape morphology. The difference in height between the bottoms of the anterior (high) and posterior (low) lingual valleys is remarkable, in particular on molars.

A fragment of the left mandible 29-2013/278 bearing p3 and p4, displays similar morphological characters (both for mandible and teeth) described for 29-2013/925. The anterior lingual valley on p4 is only slightly wider than that observed in 29-2013/278.

Isolated teeth. A left M3 29-2013/288 (K86) displays a weak paracone fold, a rather flat ectoloph profile, a single crochet, a small antecrochet, a faint crista and a mesial cingulum. The lingual side of the protocone is quite flat with a weak vertical incision.

A right M2–M3 series GMN1 29-2013/284 (K88, K89) is relatively well preserved (Fig. 4B). The ectoloph profile of
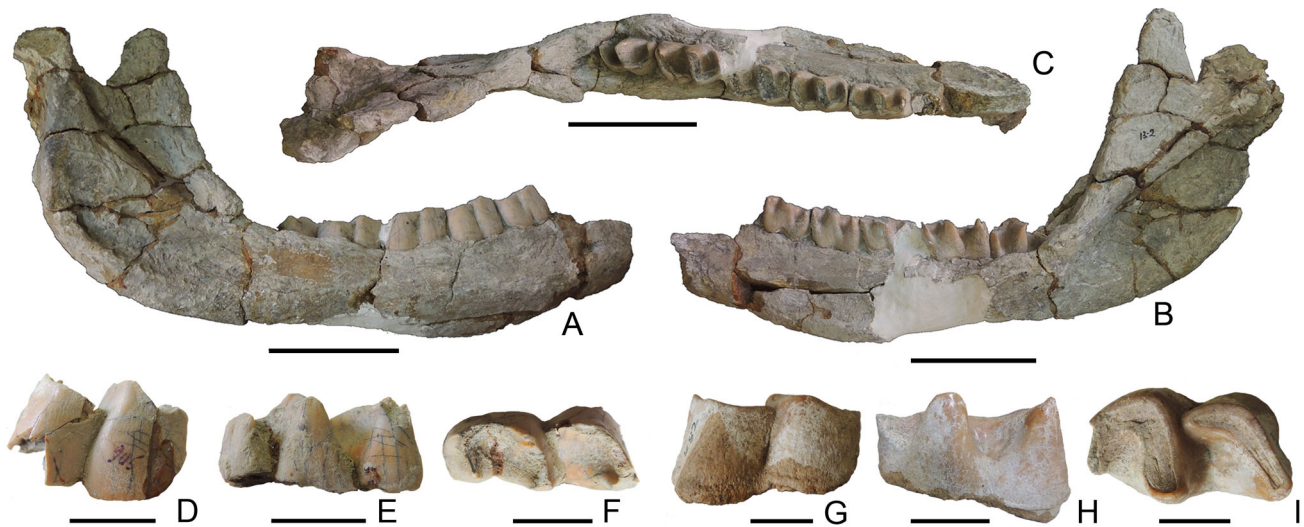
Figure 5. *Pliorhinus miguelcrusafonti* comb. nov. remains from Kvabebi. GNM1 29-2013/925 DN13-2, right hemi-mandible bearing p3–m3 in **A,** lateral; **B,** medial; **C,** occlusal views. GNM1 29-2013/282 (K905), right dp3 in **D,** buccal; **E,** lingual; **F,** occlusal views. GNM1 29-2013/279 (K82), right m3 in **G,** buccal; **H,** lingual; **I,** occlusal views. Scale bars equal 10 cm for A–C, and 2 cm for D–I.

M2 is concave in its posterior part; the paracone fold is evident and the parastyle is well developed. The median valley is partially filled by sediment, but a single crochet is obviously retained. The protoloph is anteriorly damaged. The metaloph is slightly oblique, the hypocone is not constricted and the postfossette is sub-triangular and posteriorly delimited by a cingulum. The morphology of the M3 is similar to that of GMN1 29-2013/925 and GMN1 29-2013/288 (K86); the only difference being the presence of a double antecrochet on GMN1 29-2013/284 (K88, K89).

A right P4 GMN1 29-2013/290 (K85) lacking the ectoloph bears a crista, a short crochet, a mesial cingulum, and a short lingual cingulum at the entrance of the median valley. Protocone and hypocone are joined at this stage of wear, and the postfossette is elongated.

A right D3 GMN1 29-2013/286 (K80) shows an undulated ectoloph profile, with a wide paracone fold. Metacone fold and mesostyle are present (Fig. 4C). The crochet is simple, long and curved, almost reaching the ectoloph; the metaloph is straight and the hypocone is mesially constricted. The protoloph is long and linguo-distally directed. Mesial and distal cingula are present.

A right D4 GMN1 29-2013/285 (K75) resembles in morphology the D3 GNM1 29-2013/286 (K80) except for the ectoloph that is oblique with a wide and prominent paracone fold and a faint metacone fold (Fig. 4D).

A right D4 GMN1 29-2013/287 (K79), slightly damaged on the posterior side, resembles in morphology the specimen GMN1 29-2013/285 (K75).

On the right dp3 GMN1 29-2013/282 (K905) there are no vertical rugosities or ectoloph fold on the buccal side (Fig. 5D). In buccal view, the external groove is deep and reaches the base of the crown. Cingula are absent. The tooth shows 'V'-shaped lingual valleys in lingual view (Fig. 5E). As for lower permanent teeth, the difference in height between the bottoms of the lingual valleys is marked. There is no lingual groove on the entoconid. In occlusal view (Fig. 5F), the trigonid is rather flat on its buccal side and the talonid is rounded. The entoconid is constricted whilst the metaconid is not. The paralophid is double. The protoconid fold is absent.

A right m3 GMN1 29-2013/279 (K82) displays a deep external groove (Fig. 5G) and wide 'V'-shaped lingual valleys (Fig. 5H). The difference in height between the bottoms of the valleys is as marked similarly to the m3 on the hemimandible GNM1 29-2013/925. The tooth lacks the lingual and labial cingula (Fig. 5I).

Humerus. The proximal epiphysis is damaged (Fig. 6A, B). The greater tubercle is high and strongly developed. The bone is robust (short and massive). In posterior view, the olecranon fossa is deep, with a wider than high triangular outline. In the same view, the lateral epicondyle is well developed, extending further downwards than the distal trochlea (Fig. 6A). In distal view, the lateral epicondyle is massive and rounded; the medial lip of the distal trochlea has a quite convex medial border, and it is clearly much more developed than the lateral lip of the distal trochlea; the trochlear groove is wide. In anterior view (Fig. 6B), the medial border of the medial lip of the distal trochlea is oblique if compared with the medial border of the distal epiphysis, whilst the lateral border of the lateral lip is slightly convex. The medial tuberosity on the medial-distal face is prominent. The distal trochlea is asymmetric, and the trochlear
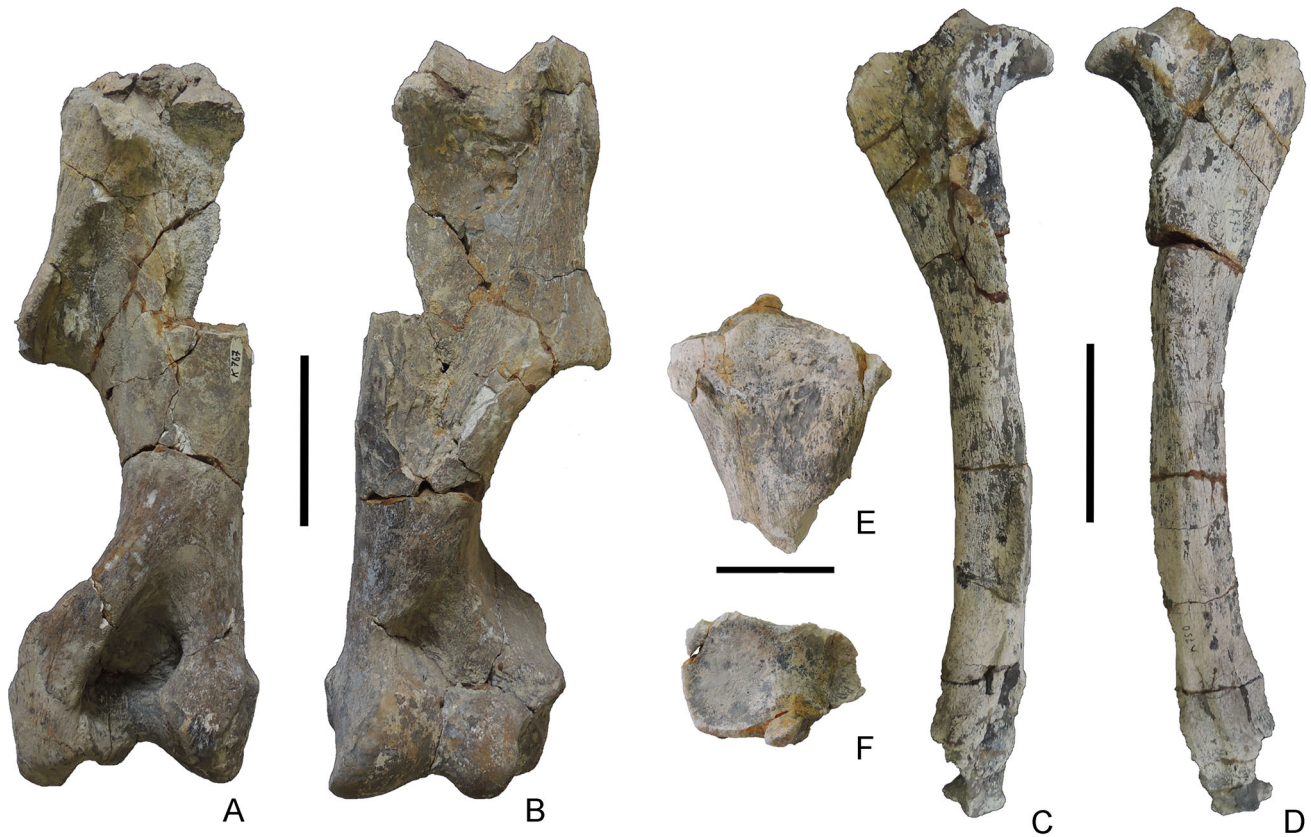
Figure 6. *Pliorhinus miguelcrusafonti* comb. nov. remains from Kvabebi. GMN1 29-2013/302 (k767), an almost complete left humerus in **A,** posterior; **B,** anterior views. GMN1 29-2013/273 (k753), an almost complete left ulna in **C,** medial; **D,** lateral views; GMN1 29-2013/276, a proximal epiphysis of a right radius in **E,** anterior; **F,** proximal views. Scale bars equal 10 cm in A–D, and 5 cm in E, F.

groove is deep (strong median constriction, 'diabolo-shaped' *sensu* Antoine 2002). The epicondylar crista is poorly developed.

Ulna. The ulna is represented by a fragment of a proximal epiphysis, a fragment of proximal epiphysis articulated with a radius, and an almost complete, but badly preserved, specimen (Fig. 6C, D). The bone is long and slender, with a narrow shaft, especially with respect to the humerus. In anterior view, the medial and lateral sides of the articular surface for the humerus are concave. The articular surfaces for the radius are represented by two surfaces slightly in contact at the level of the sigmoid incisure; the lateral one is sub-triangular and elongated towards the sigmoid incisure whereas the medial one is long and narrow. The olecranon is long and forming a closed angle with the shaft (*sensu* Antoine 2002, fig. 209b). The distal end is slender, without a strong anterolateral tubercle.

Radius. The radius is represented by three proximal epiphyses with similar morphologies: very wide proximal transverse diameter with respect to that of the diaphysis.

In anterior view (Fig. 6E, F), the coronoid process is prominent whilst the bicipital tuberosity is not particularly developed. In posterior view, the posterior proximal apophysis has two articular surfaces; the medial one is long and narrow, whereas the lateral one is higher, roundish and partially placed on the coronoid apophysis. In proximal view, the head is deep antero-posteriorly, the medial and lateral articular surfaces are sub-squared, and the lateral one is smaller and with a rounded anterior-lateral border. In the same view, the anterior border of the proximal epiphysis is concave at the level of the coronoid apophysis. The angle between the posterior border of the medial articular surface and the lateral one is obtuse.

Scaphoid. In medial view (Fig. 7A, B), the posterior border of the bone is sinuous, the magnum-facet is concave, the large articular surface for the trapezoid is saddle shaped, and the trapezium-facet delimits a straight edge. The anterior and posterior heights are equal. The anterior border of the medial side of the bone is regularly convex. In lateral view, the articular surface for
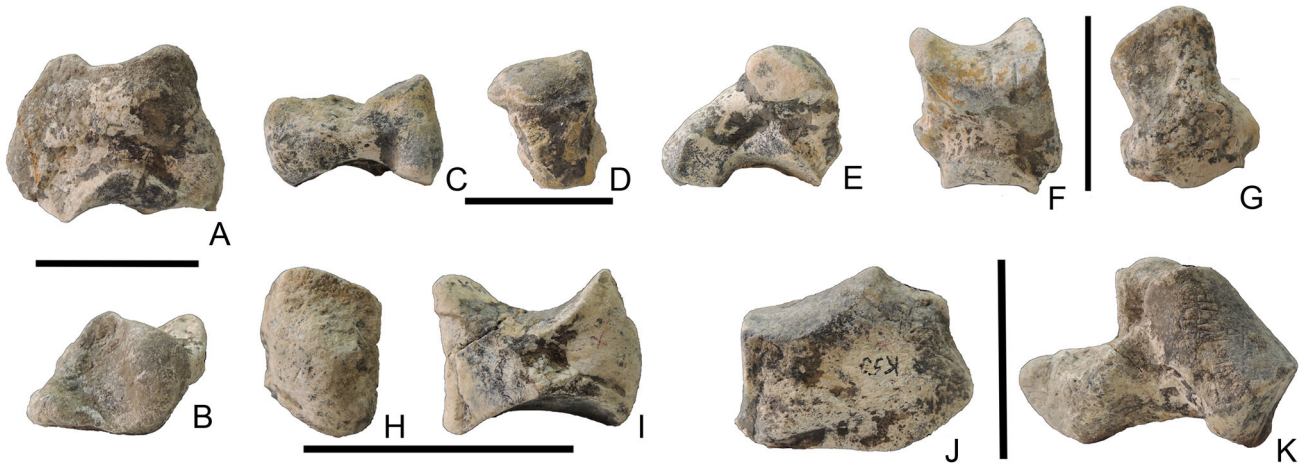
Figure 7. *Pliorhinus miguelcrusafonti* comb. nov. remains from Kvabebi. GMN1 29-2013/342 (k61), a left scaphoid in **A,** medial; **B,** proximal views. GMN1 29-2013/348 (k908), a right semilunar in **C,** proximal; **D,** anterior; **E,** medial views. GMN1 29-2013/349 (k67), a left pyramidal in **F,** anterior; **G,** medial views. GMN1 29-2013/350 (k60), a left trapezoid in **H,** anterior; **I,** lateral views. GMN1 29-2013/344 (k53), a left unciform in **J,** anterior; **K,** proximal views. Scale bars equal 5 cm.

the semilunar is connected with the proximal articular surface for the radius. Distally, another small articular surface for the semilunar is present in the anterior margin of the bone. In proximal view, the articular surface has a rhomboid shape, with a sharp anterior side and a rounded posterior side.

Semilunar. In anterior view (Fig. 7C–E), the anterior face is smooth, forming a high rectangle with a straight distal border. In proximal view, the proximal articular surface is straight in its anterior border; the articular surface for the scaphoid is well developed, and similar in length to the radius and ulna-facets. The posterior face of the bone is massive. On the medial side, there are three distinct scaphoid-facets. In distal view, the articular surface for the magnum is elongated, and it is separated from a shorter articular surface for the unciform by a marked crest.

Pyramidal. In anterior view (Fig. 7F, G), the lateral half is higher than the medial one; the medial border of the face displays a marked concavity in the middle. A developed tuberosity is present in the posterior-lateral portion of the bone. In medial view, the proximal and distal semilunar-facets are similarly developed. In the same view, the proximal articular surface is asymmetric and has a concave dorsal profile whilst the distal one is strip-shaped and symmetric (*sensu* Antoine 2002, fig. 218). The bone has an elliptic distal outline.

Trapezoid. In proximal view (Fig. 7H, I), the articular surface is sub-rectangular with a convex anterior border. In anterior view, the medial side is lower than the lateral one and the proximal and distal borders are oblique (conferring an asymmetrical outline to the bone). In

medial view, the anterior face is convex; the proximal articular surface extends towards the medial face and is connected with the distal articular surface on its posterior border.

Magnum. Two badly preserved bones are present. Only few measurements can be considered on these specimens, but their preservation state prevents any detailed description and comparison.

Unciform. In anterior view (Fig. 7J, K), the unciform displays a concave profile of the proximal articular surface and a straight medial border. The proximal lateral tuberosity is well developed and prominent. There is no posterolateral expansion on the pyramidal-facet. The latter does not join the McV-facet. The distal lateral angle on the anterior face is sharpened, testifying to the vertical orientation of the McV-facet. This orientation further points to a vestigial McV (tridactyl hand) (see Antoine 2002, p. 205 for discussion).

Second metacarpal. The bone has a slender and sub-rectilinear shaft. In proximal view (Fig. 8A–D), the articular surface for the trapezoid is wide and sub-circular. A poorly developed tuberosity occurs in the posterior end of the proximal epiphysis. In lateral view, the proximal edge is strikingly oblique with respect to the horizontal line (~45°), the articular surface for the magnum is long with a straight proximal border and a sharp median distal constriction (curved magnum-facet *sensu* Antoine 2002, fig. 228); the articular surface with the third metacarpal is small and short, restricted to the anterior half of the bone and posteriorly delimited by a marked groove (coinciding with the magnum-facet constriction). There is neither posterior Mc3-facet nor
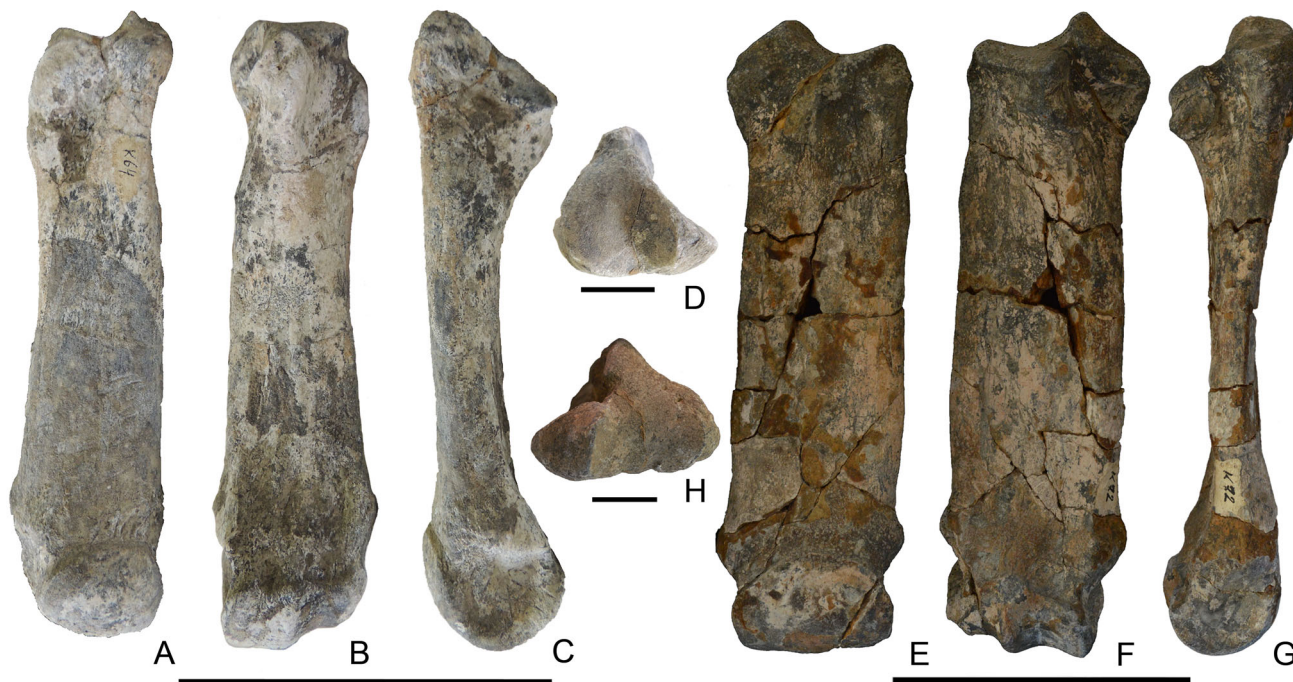
Figure 8. *Pliorhinus miguelcrusafonti* comb. nov. remains from Kvabebi. GMN1 29-2013/759 (k64), a left Mc2 in **A,** anterior; **B,** posterior; **C,** lateral; **D,** proximal views. GMN1 29-2013/758 (k72), a right Mc3 in **E,** anterior; **F,** posterior; **G,** lateral; **H,** proximal views. Scale bars equal 5 cm for A–C and E–G, and 2 cm for D and H.

delimited trapezium-facet. The intermediate relief is low and smooth.

Third metacarpal. In anterior view (Fig. 8E–H), the proximal-lateral tuberosity is prominent and the angle between its lower border and the diaphysis is obtuse. The bone is long and slender, with medial and lateral sides parallel in anterior view, and unwidened proximal and distal ends. In proximal view, the articular surface for the magnum shows a sub-triangular shape and it is anteroposteriorly wide, reaching more than half of the lateral border. The anterior border of the proximal epiphysis is sinuous. In lateral view, the posterior proximal surface is higher than wide, with a distal convex border; it is separated from the anterior-lateral surface by a wide groove. The diaphysis is concave in the middle of its posterior border, but there is no tubercle. The intermediate relief is low and smooth. Both metacarpals have a flat insertion for the m. extensor carpalis and a long insertion for the m. interossei.

Tibia. An almost complete tibia is preserved (Fig. 9A–D). In proximal view, the tibial tuberosity is rounded, and the tibial groove is wide and very shallow. The tibial spine is prominent, and the central intercondyloid area has a 'V'-shaped morphology and is posteriorly closed. The lateral articular surface is wide, whilst the medial articular surface is smaller and less elongated than the former. The proximal fibula-facet is located

high, almost joining the femur-facet. In distal view, the lateral distal articular surface is sub-elliptical, and the medial one is sub-trapezoidal and quite flat. The medial and posterior borders of the distal epiphysis are concave (groove for the tendon of the m. tibialis posterior). Distally, the posterior apophysis is low and rounded.

Astragalus. The astragalus (Fig. 10A, B) is badly preserved and the posterior articular surfaces are covered by encrusted sediment. It is roughly square in anterior view (TD/H = 1.07) and it is robust in medial view (DAP/H = 0.69). In anterior view, the trochlea is large and asymmetric, with a deep median constriction. The posterior edge is nearly straight. The medial lip is very narrow whilst the lateral lip is particularly wide and globular. The fibula-facet is flat, narrow and vertical. The collum tali (= neck) is high and deep. The medial tuberosity (partially damaged) is particularly low and not prominent at all, i.e. very close to the distal border of the medial face. In distal view, the axis of the trochlea is oblique with respect to that of the cuboid + navicular-facets (~30° angle). There is a posterior stop on the cuboid-facet.

Calcaneum. The bone is robust, with a massive tuberosity and a sustentaculum tali (=sustentacular process) curved transversally (concave anteriorly). In lateral view (Fig. 10C, D), the posterior border of the bone is slightly concave, and the tuber extends a little bit more forward than the beak (*sensu* Guérin 1980, fig. 22). The articular

Figure 9. *Pliorhinus miguelcrusafonti* comb. nov. remains from Kvabebi. GMN1 29-2013/752 (k533), a right tibia in **A,** anterior; **B,** posterior; **C,** proximal; **D,** distal views. Scale bar equals 10 cm.

surface located on the sustentaculum tali is separated from the proximal lateral articular surface for the astragalus by a marked and narrow groove. In distal view, the articular surface for the cuboid is wide, anteriorly narrower, and shows a marked concavity in the posterior border. The cortical surface is damaged. Nevertheless, it seems that the tibia- and fibula-facets are absent and that the insertion for the m. fibularis longus is not prominent at all.

Third metatarsal. The bone is badly preserved; in proximal view, the proximal articular surface has a convex anterior border, whereas the lateral proximal

articular surfaces are anteroposteriorly compressed. The bone lacks the distal epiphysis.

Fourth metatarsal. Only the proximal epiphysis of MtIV is preserved (Fig. 11A–C). In proximal view, the articular surface is sub-circular. Posteriorly, this surface is bordered by a thick and continuous unarticulated pad-shaped tuberosity separated by a faint groove. On the medial side of the bone, the posterior articular surface for the third metatarsal is quite rounded and well separated from the (damaged) anterior one. In proximal view, both facets form a *c.* 105° angle. The shaft was well curved (convex medially) and the proximal head was not widened with respect to the shaft. The insertion for the m. interossei is long (i.e. running along the proximal half of the shaft).

Results

Morphological comparison
Cranial remains. Compared with the studied material, the skull of *S. jeanvireti* from Milia (Greece; Guérin & Tsoukala 2013, fig. 3A–C) displays a longer neurocranial portion with wider post-orbital constriction and well-marked frontal-parietal crests. In lateral view, in *S. jeanvireti* from Milia the dorsal profile of the skull is less concave, and the parietal bones are flatter than in the skull from Kvabebi. Further, the Milia specimen (Guérin & Tsoukala 2013, fig. 3C) has the posterior border of the zygomatic arch higher than in the Kvabebi specimen. The nuchal crest on the Milia skull, in occipital view (Guérin & Tsoukala 2013, fig. 3F), is more massive and with rounded borders in respect to the specimen from Kvabebi. The skull NMB Vt2 from Vialette (France), also assigned to *S. jeanvireti*, has a sub-trapezoidal occipital face, and the parietal bones are rather flat, contrary to the skull from Kvabebi. The infraorbital foramen, the posterior border of the nasal notch and the anterior border of the orbit, are more anteriorly placed in *S. jeanvireti* than in Kvabebi skull. The upper teeth from Kvabebi mainly differ from those of *S. jeanvireti* by having multiple enamel folds on the premolars.

The skulls of *S. etruscus* from Upper Valdarno differ from those of Kvabebi in having a more advanced position of the foramen infraorbitalis and of the anterior border of the orbit, and in having a flat dorsal profile. In addition, the occipital face in *S. etruscus* is trapezoidal in shape, with the width of the nuchal crest shorter than the width at the mastoids. The upper premolars of *S. etruscus* differ from those of Kvabebi in lacking multiple crochets, and in having a less prominent paracone fold and a less wavy ectoloph profile.

Figure 10. *Pliorhinus miguelcrusafonti* comb. nov. remains from Kvabebi. GMN1 29-2013/761 (k901), a right astragalus in **A,** anterior; **B,** distal views. GMN1 29-2013/756 (k69), a left calcaneus in **C,** lateral; **D,** anterior views. Scale bars equal 5 cm.
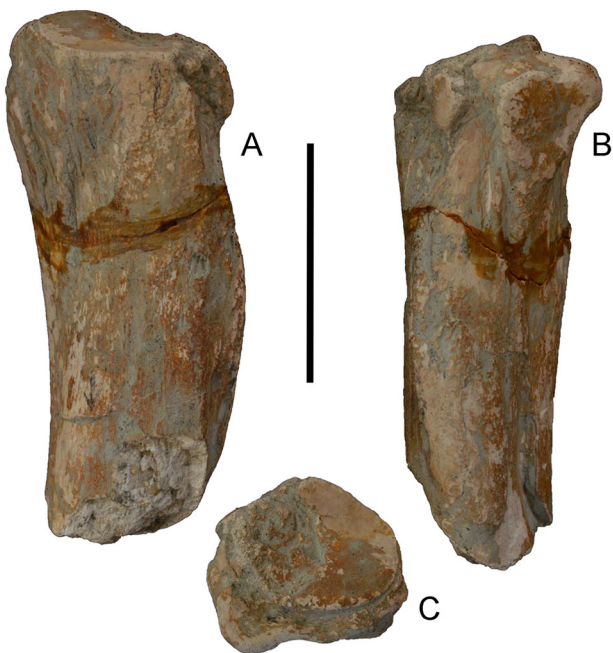

Figure 11. *Pliorhinus miguelcrusafonti* comb. nov. remains from Kvabebi. GMN1 29-2013/934 (k73), a proximal fragment of right Mt4 in **A,** anterior; **B,** lateral; **C,** proximal views. Scale bar equals 5 cm.

The skull of '*D.*' *bethlehemsis* differs from the studied specimens in having a straight posterior profile of the nuchal crest in dorsal view, and in having a less massive neurocranial portion. In addition, the upper teeth of '*D.*' *bethlehemsis* are characterized by closed medifossettes, joined protocone and metacone on the premolars, and a circular postfossette on the premolars.

The neurocranial portion GNM1 29-2013/300 (K744) from Kvabebi resembles that of *P. megarhinus* from Saint-Laurent-des-Arbres (France; Guérin *et al.* 1969, fig. 6) even if the parietals are narrower in the former. In dorsal view, the posterior border of the nuchal crest is somewhat more concave in the skull from Kvabebi than in that from Saint-Laurent-des-Arbres. In occipital face view, the skull from Saint-Laurent-des-Arbres displays a trapezoidal shape, whilst in Kvabebi it is rather squared. The mandible from Kvabebi displays a deeper sigmoidal incisure and a more convex mandibular angle in respect to the mandible from Saint-Laurent-des-Arbres (Guérin *et al.* 1969, fig. 8). Compared with the studied remains, the lower premolars from Saint-Laurent-des-Arbres (Guérin *et al.* 1969, figs 13–16) display a shorter trigonid in occlusal view and mesial and distal cingula.

Contrary to the studied specimens, the upper premolars from Kávás (Hungary; Pandolfi *et al.* 2015) lack lingual cingula, they display a wavy profile of the ectoloph, and the molars have a developed parastyle. Furthermore, the skull from Kávás differs from the Kvabebi specimen in having a higher and trapezoidal-shaped occipital face.

The skull from Lens Lestang (France; *P. megarhinus*) differs from the studied material in having flatter parietal bones, a poorly developed nuchal crest, upper premolars with a continuous lingual cingulum and a single crochet. Compared with the upper teeth from Kvabebi, the M2 from Lens Lestang has a faint mesostyle and the M1 displays a less developed metastyle and a narrower parastyle. The M3 from Lens Lestang is larger than that from Kvabebi, with a simple crochet and a more developed parastyle that overhangs the metastyle of M2; the latter features can be also observed on the M3s from Montpellier assigned to the same species (Guérin 1980, pls. 10, 15).

The neurocranial portion of the skull from Montpellier (*P. megarhinus*) is similar to that from Lens Lestang, with flat parietals, a nuchal crest poorly developed posteriorly, and a zygomatic arch more highly placed in respect to the skull from Kvabebi. Contrary to the specimens from Kvabebi, the crochet on P2 and P3 from Montpellier is single, and a quite continuous lingual cingulum is present on the upper premolars. Furthermore, in the upper teeth from Montpellier (Guérin 1980, pls. 10, 15), the metastyle and parastyle on P3 are less developed and the ectoloph on M1 and M2 is shorter than in Kvabebi.

The rhinoceros from Kvabebi differs from *P. miguelcrusafonti* from Layna in lacking additional faint internal folds (antecrochet and crista) on D4. Anyway, the scanty material referred to the Layna species does not allow an exhaustive comparison. The P3 from Layna is an isolated unworn tooth; it closely resembles the P3 from Kvabebi, differing only by the presence of a faint metacone fold (subject to variation with wear). A partially preserved M1 from Layna displays a small crochet and antecrochet, contrary to what is observed on the M1 from Kvabebi; these two folds are in any case well documented in some upper molars from Montpellier assigned to *P. megarhinus*, suggesting intraspecific variability for these characters, as reported by Guérin (1980). Similarly, internal folds, such as a crista, are present on the M2 from Layna as well as on some M2s from Montpellier (France). Similarly to the Kvabebi tooth, the lower molars from Layna show an obtuse angle between the lophids in occlusal view, a deep external groove that reaches the base of the crown, 'V'-shaped lingual valleys, great difference in height

between the bottoms of the lingual valleys and absence of lingual and buccal cingula. The same morphologies are shared between the m2s from Kvabebi and Layna. The lower premolars on the holotype from Layna are similar to those on the mandible from Kvabebi in lacking buccal and lingual cingula, in having a narrow angle between the trigonid and talonid, 'V'-shaped lingual valleys, great difference in height between the bottoms of the valleys, and a deep external groove.

Postcranial remains. In distal view, the lateral epicondyle on the humerus is massive and squared in Kvabebi, massive and rounded in *P. megarhinus*, and rounded in *S. etruscus* and *S. jeanvireti*. In the same view, the anterior border of the lateral lip of the trochlea is wide and straight in Kvabebi and *S. etruscus*, narrow and rounded in *S. jeanvireti* and wide and rounded in *P. megarhinus*. In anterior view, the medial tuberosity on the distal epiphysis is prominent in the specimen from Kvabebi and poorly developed on the other species. In the same view, the medial border of the medial lip of the trochlea is oblique in the Kvabebi specimen and in *S. etruscus* whilst it is parallel to the medial border of the distal epiphysis in *S. jeanvireti* and *P. megarhinus*. In posterior view, the olecranial fossa is narrow in Kvabebi, *P. megarhinus* and *S. jeanvireti* and wide in *S. etruscus*.

On the radius, in anterior view, the insertion of the brachial biceps is medially placed in the Kvabebi radii as well as on the rhinoceros from Layna and *S. etruscus*. In *P. megarhinus* the brachial biceps is centred on the proximal epiphysis whilst on *S. jeanvireti* it is slightly medially placed. The proximal profile of the lateral articular surface, in anterior view, is almost perpendicular to the main axis of the bone in *P. miguelcrusafonti* and Kvabebi, it forms an acute angle in *S. jeanvireti* and *P. megarhinus* and is concave in *S. etruscus*.

The proximal articular surface of the ulna is transversally wide in Kvabebi and *P. miguelcrusafonti* and narrower in *P. megarhinus*, *S. jeanvireti* and *S. etruscus*. The articular surfaces for the radius are in contact in Kvabebi and separated in *P. megarhinus*, *S. jeanvireti* and *S. etruscus*. The asymmetry of the anconeal process is strong (laterally higher) in Kvabebi, *P. miguelcrusafonti*, *P. megarhinus* and *S. jeanvireti* and weak in *S. etruscus*.

In medial view, the anterior border of the scaphoid is regularly convex in Kvabebi and *P. miguelcrusafonti* whilst the anterior tuberosity is well developed and clearly separated from the distal articular surface in *P. megarhinus*, *S. jeanvireti* and *S. etruscus*. The posterior border of the bone, in medial view, is sinuous in Kvabebi and *P. miguelcrusafonti*, slightly concave in *P. megarhinus* and slightly concave or straight in *S.*

jeanvireti and *S. etruscus*. The proximal articular surface is similar in size and proportions in Kvabebi and *P. miguelcrusafonti*, whilst it is wider in *P. megarhinus* and *S. jeanvireti*. In *S. etruscus*, the maximum width of the proximal articular surface is similar to the width of the anterior border of the bone.

The anterior dorsal face of the semilunar is low and wide in Kvabebi and *S. etruscus*, high and wide in *P. megarhinus*, and high and narrow in *S. jeanvireti*. The proximal profile of the bone, in medial view, is straight in Kvabebi and sinuous in *P. megarhinus* and *S. etruscus*. In distal view, the posterior profile of the bone is strongly asymmetric in Kvabebi and straight in *P. megarhinus* and *S. etruscus.*

On the pyramidal, the heights of the anterior and posterior faces are similar in Kvabebi, *P. miguelcrusafonti*, and *S. etruscus*, whilst in *P. megarhinus* the anterior face is higher than the posterior one and in *S. jeanvireti* the posterior face is higher than the anterior one. The tuberosity on the lateral face is weakly developed in Kvabebi and *P. miguelcrusafonti* and well developed in other species. The distance between the distal and proximal articular surfaces on the medial face is high in the Kvabebi specimen, in *P. miguelcrusafonti*, *P. megarhinus* and *S. eanvireti*, whilst it is low in *S. etruscus*.

The posterior border of the trapezoid, in medial view, is straight in Kvabebi and *P. miguelcrusafonti* and convex in *S. jeanvireti*. In the same view, the anterior border of the proximal articular surface ends before the anterior face of the bone in Kvabebi and *P. miguelcrusafonti* and overhangs the anterior face in *S. etruscus.*

The magnum from Kvabebi is badly preserved and useful morphological characters for comparison cannot be detected.

The unciform displays, in anterior view, a concave profile of the proximal articular surface in Kvabebi and a straight profile in all other species. The proximal lateral tuberosity is well developed and prominent in Kvabebi and *P. megarhinus*, poorly developed in *S. jeanvireti* and well developed in *S. etruscus*. The distal lateral angle on the anterior face is sharpened in Kvabebi and *S. etruscus* and rounded in *P. megarhinus* and *S. jeanvireti*.

The McII from Kvabebi displays a concave lateral border in proximal view as well as the species from Layna and *P. megarhinus*, whilst it is straight in *S. jeanvireti* and *S. etruscus*. In Kvabebi, the length and width of the proximal articular surface are similar in dimensions. In *S. jeanvireti* the articular surface is longer than wide as well as in *P. megarhinus* whilst in *S. etruscus* it is wider than long. In lateral view, the distal border of the proximal lateral articular surface is concave in Kvabebi, *P. miguelcrusafonti* and *P. megarhinus* whilst

it is straight in *S. jeanvireti* and *S. etruscus*. In the same view, the distal portion of the proximal lateral articular surface is small and posteriorly delimited by a marked groove in Kvabebi, *P. miguelcrusafonti* and *P. megarhinus*. In *S. etruscus* and *S. jeanvireti* the distal portion of the proximal lateral articular surface is posteriorly delimited by a faint groove.

On the McIII, the section of the diaphysis in Kvabebi and *P. miguelcrusafonti* displays a marked concavity in its posterior border, whilst it is rather straight or slightly concave in *P. megarhinus* and *S. jeanvireti* and straight in *S. etruscus*. In proximal view, the proximal lateral articular surfaces are similar in length in *S. etruscus* and *S. jeanvireti*, whilst in Kvabebi, *P. miguelcrusafonti* and *P. megarhinus* the anterior surface is longer than the posterior one. In the same view, the posterior articular surface for the McIV is partially visible in *S. etruscus* and *S. jeanvireti* and it is not visible in Kvabebi and *P. megarhinus*. The anterior border of the proximal epiphysis is sinuous in Kvabebi, *P. miguelcrusafonti* and *S. jeanvireti* whilst it is slightly concave or straight in *P. megarhinus* and slightly convex in *S. etruscus*.

In proximal view, the anterior groove on the proximal epiphysis of the tibia is wide and deep in the Kvabebi specimen and in *P. megarhinus*, and wide and shallow in *S. jeanvireti* and *S. etruscus*. The anterior tuberosity is slender and long in Kvabebi, short and massive in *P. megarhinus* and *S. etruscus* and prominent and rounded in *S. jeanvireti*. The interspine groove is deep and 'V'-shaped in Kvabebi, narrow and posteriorly open in *P. megarhinus*, shallow and posteriorly open in *S. etruscus* and wide and deep and posteriorly open in *S. jeanvireti*. In proximal view, the medial articular surface is less developed than the medial side of the proximal epiphysis in the Kvabebi specimen; this surface reaches the anterior border of the proximal epiphysis in *P. megarhinus*, *S. etruscus* and *S. jeanvireti*. In distal view, the posterior lateral tuberosity is prominent and rounded in Kvabebi and *P. megarhinus*, and poorly developed in *S. etruscus* and *S. jeanvireti*. The posterior border of the distal articular surface is strongly concave in the Kvabebi specimens; it is regularly concave in *S. jeanvireti*, and slightly concave in *S. etruscus* and *P. megarhinus*.

The astragalus from Kvabebi is badly preserved, thus preventing a detailed morphological comparison. Contrary to *S. etruscus*, in the specimen from Kvabebi the collum tali is high and the posterior stop on the cuboid-facet is present. These characters are shared with *P. miguelcrusafonti*, *P. megarhinus* and *S. jeanvireti*. The morphology of the articular facets for the calcaneus cannot be observed on the Kvabebi astragalus.

Table 2. Comparative table of Pliocene–earliest Pleistocene Rhinocerotidae skulls from Northern Eurasia. Data from direct observations and Guérin (1972, 1980), Guérin & Tsoukala (2013), Pandolfi *et al.* (2020).

Measurements in mm	n° in Guérin, 1980	Kvabebi GMN1 29-2013/ 925 DN229	Kvabebi GMN1 29-2013/ 300 (k744)	'D.' bethlehemsis	S. etruscus	S. jeanvireti	P. megarhinus
Width of the occiput	15		*c.* 164	165.32	101–174	110–148	165–200
Width of the skull at the mastoid apophyses	16	*c.* 235	231.5		158–228	234–253	243–282
Minimal distance between the fronto-parietal crests	17			49.25	34–60.5	48	43.5–69
Width at the preorbital processes	20			170	162–224	217–221	210–264
Maximal width at the zygomatic arcs.	21				253.5–324	364–372	311–364
Distance of the foramen magnum to the occipital crest	23		141	120.63	117–153		167–190
Width of the foramen magnum	31		*c.* 46	48.26	40–57.5	58	72
Width of the occipital condyles	32	121.01	133.16	116.26	103–134		127–158
Width of the nasals	33			105.74			

In the calcaneus from Kvabebi, in posterior view, the sustentaculum tali forms an obtuse angle with the main axis of the bone and it is medially rounded and bends downwards, as in *P. miguelcrusafonti*. In the same view, the lateral border of the bone is concave in Kvabebi, *P. megarhinus* and *P. miguelcrusafonti* and straight in *S. etruscus* and *S. jeanvireti*. In *P. megarhinus* the sustentaculum tali is almost perpendicular to the main axis of the bone and it is medially squared and enlarged. In *S. jeanvireti* the sustentaculum talii has an obtuse angle with the main axis of the bone and it is medially squared and enlarged whilst in *S. etruscus* it is almost perpendicular to the main axis of the bone and medially rounded. In lateral view, the posterior border of the bone is regularly concave in Kvabebi, slightly concave or straight in *S. etruscus* and *P. megarhinus* and slightly convex in *S. jeanvireti*. In distal view, the proximal articular surfaces for the astragalus are in contact in Kvabebi, in contact or separated by a shallow groove in *S. etruscus* and separated by a marked groove in *P. megarhinus* and *S. jeanvireti*.

Discriminant morphological characters cannot be detected on MtIII due to the bad state of preservation of the material from Kvabebi.

On the MtIV, in medial view, the posterior proximal articular surface is rectangular-shaped, with the main axis parallel to the main axis of the bone as well as in *P. miguelcrusafonti*. In *P. megarhinus* this surface is sub-circular. In *S. jeanvireti*, the articular surface is sub-elliptical in shape and its main axis is oblique in respect

to the bone as well as in *S. etruscus*. In proximal view, the proximal articular surface is less developed than the proximal epiphysis in Kvabebi, *P. miguelcrusafonti* and *P. megarhinus*. Proximal epiphysis and proximal articular surface are almost similar in *S. jeanvireti* and *S. etruscus*. In addition, the posterior border of the proximal articular surface is regularly bordered by a not-articular surface in Kvabebi and *P. miguelcrusafonti*, weakly bordered by an unarticulated surface in *P. megarhinus* and *S. etruscus* and partially bordered by an unarticulated surface in *S. jeanvireti*.

Morphometric comparison

The dimensional characters of the specimens from Kvabebi have been compared with several measurements of different Pliocene and Early Pleistocene species collected from Eurasian localities. The considered data are from previous studies and direct observations (the comparative tables are reported in Supplemental Tables S3–S16). The few measurements available on the skulls (Table 2) revealed that the width of the occiput is larger than *S. jeanvireti*, slightly smaller than *P. megarhinus* and similar to 'D.' bethlehemsis, whilst the width at the mastoid is smaller than *S. jeanvireti* and *P. megarhinus* and larger than *S. etruscus*. The height of the occipital face is smaller than in *P. megarhinus* and the total length of the upper toothrow is close to the estimated values of 'D.' bethlehemsis and the maximal

Table 3. Comparative table of Pliocene–earliest Pleistocene Rhinocerotidae upper toothrow from Northern Eurasia. Data from direct observations and Guérin (1972, 1980), Pandolfi *et al.* (2020).

Tooth row	Ltot	LM	LP	LP3–P4
Kvabebi GMN1 29-2013/925 DN229	242.5	148.82	112.48	82.61
P. megarhinus	255–274	142–162.5	105.5–128	74–97
S. jeanvireti	248	134–145	115.5	77–83
S. etruscus	220–245	126–145	100–135	67–83.5

Table 4. Comparative table of Pliocene–earliest Pleistocene Rhinocerotidae lower toothrow from Northern Eurasia. Data from direct observations and Guérin (1972, 1980), Pandolfi *et al.* (2020).

Tooth row	Ltot	Lm	Lp	Lp3–p4
Kvabebi	*c.* 241	139.67	*c.* 104	72.68
P. miguelcrusafonti			103	70.5
P. megarhinus	228–293	134–165	101–136	71–91
S. jeanvireti	234–242	127–138	98–106	69.5–77
S. etruscus	210–251.5	121–143	87–108	63–80.5

values of *S. etruscus*; they all are smaller than *P. megarhinus* (Table 2).

The length of the upper molars (Table 3) of Kvabebi is slightly larger than *S. etruscus* and *S. jeanvireti*. The P2 from Kvabebi is slightly longer than *S. etruscus* and *S. jeanvireti* as well as M1 and M2, which are close to the values of *P. miguelcrusafonti* from Layna. The dimensions of the lower teeth (Table 4) from Kvabebi are close to those of *P. miguelcrusafonti* from Layna and they also fall within the variability of other Pliocene taxa.

The diaphysis of the humerus from Kvabebi falls between the largest *S. etruscus* specimens and the smallest ones of *S. jeanvireti*, whilst humeri of *P. megarhinus* are characterized by a wider and deeper diaphysis (Table S3). Considering the transverse diameter of the trochlea and the anteroposterior diameter of the distal epiphysis (Supplemental Table S3), the specimen from Kvabebi falls among the largest representatives of *S. etruscus*, being much smaller than the considered specimens of *S. jeanvireti* and *P. megarhinus*. The same result is obtained considering the maximal transverse and anteroposterior values of the distal epiphysis (Supplemental Table S3).

The proximal epiphysis of the radius (Supplemental Table S4) from Kvabebi is smaller than in *S. jeanvireti* and *P. megarhinus* and, similarly to the humerus, falls within the largest considered *S. etruscus* specimens. The measurements of the two radii collected at Perpignan (France) and assigned as *P. miguelcrusafonti* by Guérin & Santafé-Llopis (1978) are included within the range size of *P. megarhinus*. It should be noted that only one of the two radii from Perpignan was later reported as belonging to *P. miguelcrusafonti* by Guérin (1980, n°40931). The values of the distal epiphysis of radius

from Kvabebi fall again within the maximal values of *S. etruscus* and are smaller than those of other Pliocene rhinoceroses (Supplemental Table S4), including *P. miguelcrusafonti* from Perpignan. A distal epiphysis of a radius from Layna (MNCN 23828), not included in the study of Guérin & Santafé-Llopis (1978), is close in size to that from Kvabebi (Supplemental Table S4), suggesting that the concerned specimens from Perpignan should be re-assigned to *P. megarhinus*.

The few available measurements of the ulna (Supplemental Table S5) only suggest that the specimens from Kvabebi are a little larger than those of *S. etruscus* and somewhat smaller than in *S. jeanvireti*.

The scaphoid from Kvabebi approximates in size the specimen from Layna (Supplemental Table S6); it is longer and higher than in *S. etruscus*. In addition, the studied specimen is shorter and lower than in *S. jeanvireti* and has a less developed proximal articular surface in respect to *P. megarhinus* (Supplemental Table S6).

The unciform from Kvabebi, larger than in *S. etruscus*, falls within the range size given by Guérin (1980) for the Pliocene species (Supplemental Table S7).

The semilunar from Kvabebi is longer and higher than in *S. etruscus* and it is close to the minimal length values given by Guérin (1980) for the Pliocene species (Supplemental Table S8).

The pyramidal from Kvabebi is close in size to the specimens from Layna and to the minimal values of *P. megarhinus*. The studied specimen is longer than in *S. etruscus* and somewhat lower and narrower than in *S. jeanvireti* (Supplemental Table S9).

The trapezoid from Kvabebi is close in size to the specimen from Layna (Supplemental Table S9); it is smaller than in *P. megarhinus* and *S. jeanvireti*.

Concerning the McII, the specimens from Layna and Kvabebi show similar values (Supplemental Table S10). The McIIs from Layna and Kvabebi are close to the maximal values of *S. etruscus* and the minimal ones of *S. jeanvireti* (Supplemental Table S10). The McII for Perpignan, previously assigned to *P. miguelcrusafonti*, is larger than both specimens of *P. miguelcrusafonti* from Layna (for which the maximal length is lacking) and the one from Kvabebi (Supplemental Table S10). The McII from Perpignan is the only one listed in Guérin (1980) as belonging to *P. miguelcrusafonti*; we consider here
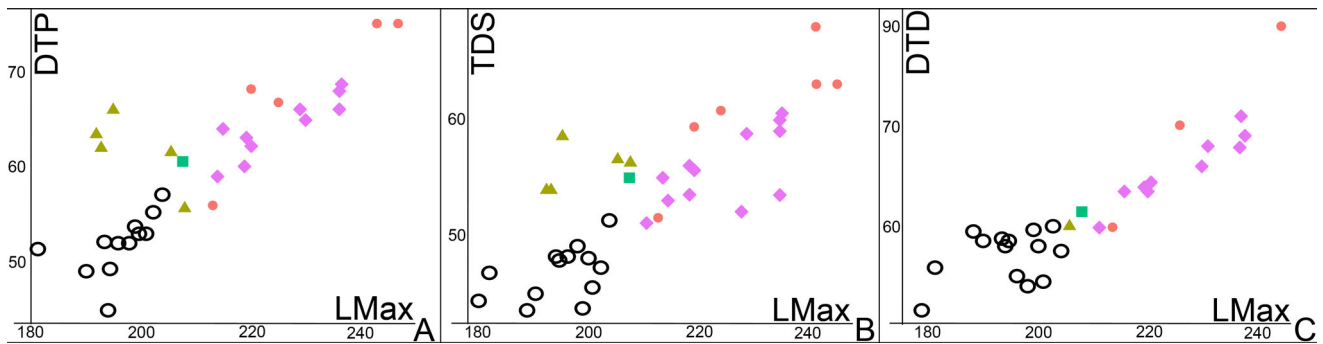
Figure 12. Scatterplots showing the relationships between the maximal length (LMax). **A,** the proximal transverse diameter (DTP); **B,** the transverse diameter of the diaphysis (TDS); **C,** the distal transverse diameter (DTD) in the Mc3s of the considered Pliocene taxa. Empty circle = *S. etruscus*; triangle = *P. miguelcrusafonti*; filled square = Kvabebi; filled circle = *P. megarhinus*; filled rhombus = *S. jeanvireti*.
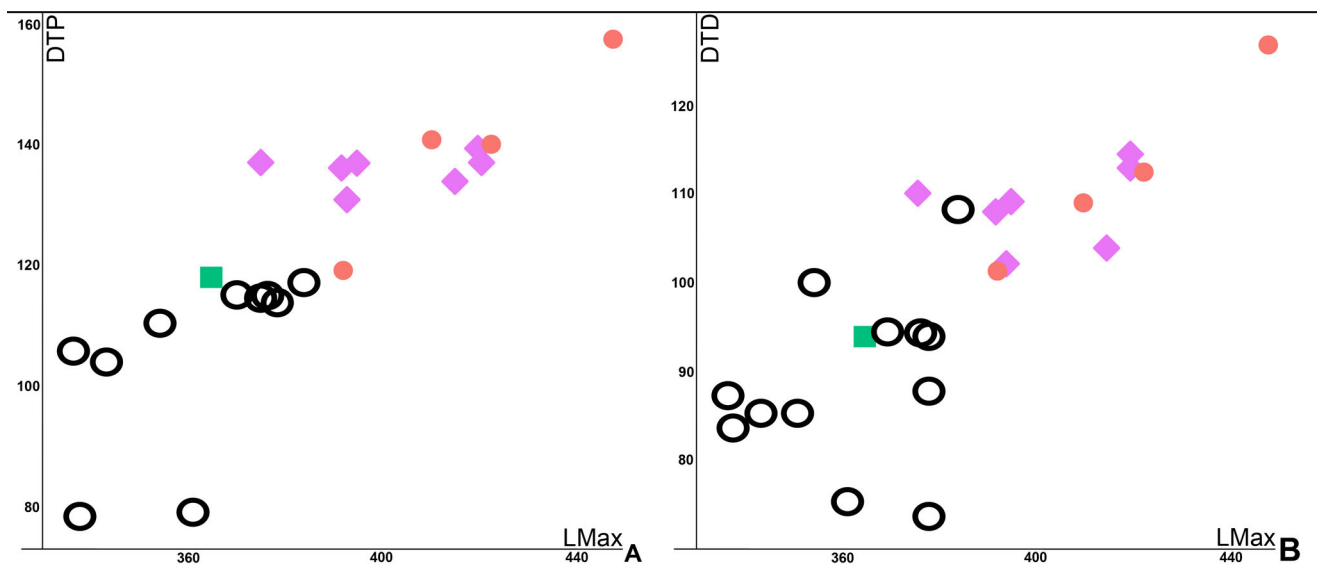

Figure 13. Scatterplots showing the relationships between the maximal length (LMax). **A,** the proximal transverse diameter (DTP); **B,** the distal transverse diameter (DTD) in the tibias of the considered Pliocene taxa. Empty circle = *S. etruscus*; triangle = *P. miguelcrusafonti*; filled square = Kvabebi; filled circle = *P. megarhinus*; filled rhombus = *S. jeanvireti*.

the two McIIs from Layna as certainly belonging to this taxon and regard the specimen from Perpignan as possibly referable to *P. megarhinus*.

Considering the maximal length and the diameter of the proximal epiphysis of the McIII (Fig. 12A; Supplemental Table S10), the Kvabebi sample is close to the largest specimens of *S. etruscus* and the smallest specimens of *S. jeanvireti*. This result is also evident considering the maximal length and the transverse diameter of the diaphysis (Fig. 12B), and the distal transverse diameter (Fig. 12C). The specimens from Kvabebi and *P. miguelcrusafonti* are morphometrically different from other species considered in the values of the transverse and anteroposterior diameters of the proximal epiphysis (Supplemental Table S11).

The size of the tibia from Kvabebi falls within the largest specimens of *S. etruscus*; the studied specimen is smaller than in *S. jeanvireti* and *P. megarhinus* (Fig. 13; Supplemental Table S12).

The astragalus from Kvabebi is badly preserved and several measurements cannot be considered (Supplemental Table S13). The plots reported in Figure 14 show that the specimen from Kvabebi falls with the largest *S. etruscus* specimens and that it is somewhat smaller than *S. jeanvireti* and *P. megarhinus*.

The dimensions of the calcaneus from Kvabebi are close to those of the specimen from Layna and both fall within the largest representatives of *S. etruscus*. They are somewhat smaller than in *S. jeanvireti* and *P. megarhinus* (Supplemental Table S14).
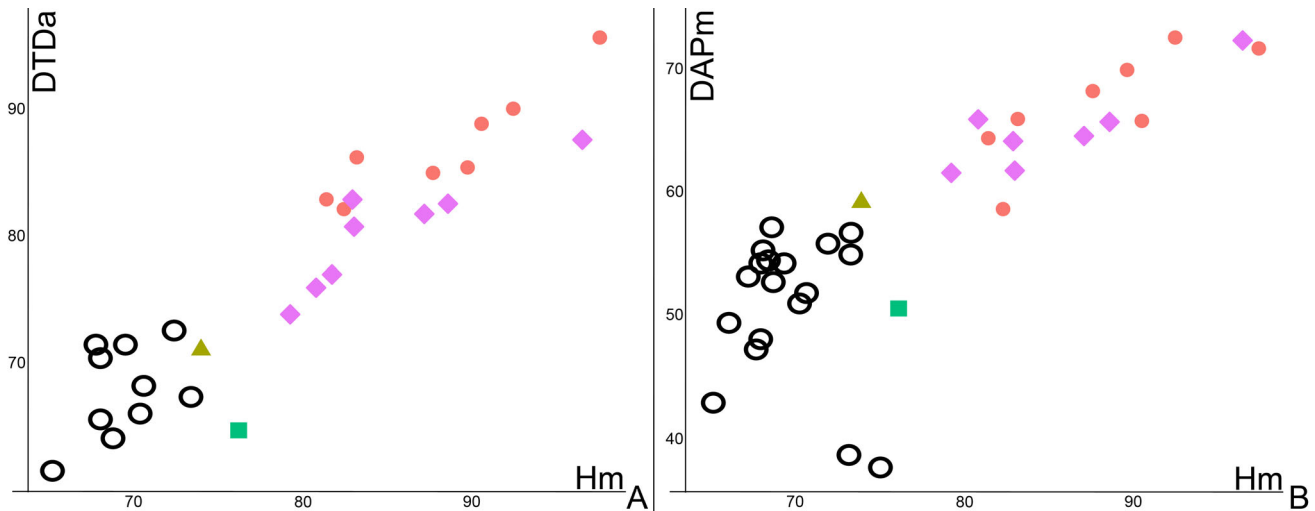
Figure 14. Scatterplots showing the relationships between the medial height (Hm). **A,** the articular distal transverse diameter (DTDa); **B,** the medial anteroposterior diameter (DAPm) in the astragali of the considered Pliocene taxa. Empty circle = *S. etruscus*; triangle = *P. miguelcrusafonti*; filled square = Kvabebi; filled circle = *P. megarhinus*; filled rhombus = *S. jeanvireti*.

Phylogenetic analysis

A cladistic analysis is here performed in order to investigate the phylogenetic relationships of the Kvabebi rhinoceros and of other Pliocene Eurasian rhinocerotines.

A first analysis was run with 280 characters scored in 31 terminal taxa, i.e. with the Kvabebi rhino and *Dicerorhinus miguelcrusafonti* considered a priori as distinct terminals (Supplemental texts S2–S4). Five most-parsimonious trees are retrieved (tree length = 1316 steps, consistency index = 0.282, retention index = 0.479, homoplasy index = 0.718), with the latter terminals being sister taxa, with a good support (Bremer index = 3; Supplemental text S3), especially given the low number of anatomical elements directly comparable between Layna and Kvabebi samples. Moreover, this clade (considered here as defining *Pliorhinus miguelcrusafonti*) is sister taxon to *Pliorhinus megarhinus*, with a very strong support (Bremer index = 6; Supplemental text S3).

Accordingly, we have performed a second analysis, with Layna and Kvabebi samples merged into *Pliorhinus miguelcrusafonti*. This analysis is therefore

based on 280 characters scored in 30 terminal taxa (Supplemental text S4). The same five most-parsimonious trees are retrieved, as reported in Supplemental text S4. The consensus tree is shown in Figure 15 (tree length = 1349 steps, consistency index = 0.274, retention index = 0.451, homoplasy index = 0.726). The suprageneric relationships here detected within Rhinocerotidae are in agreement with previous analyses based on morpho-anatomical characters (e.g. Antoine 2002; Antoine *et al.* 2010, 2021). In the obtained tree, the Rhinocerotina clade (node 1: supported by eight unambiguous synapomorphies) includes all the extant species and their fossil relatives; the general topology is similar to those reported and discussed by Antoine *et al.* (2021). Two major clades can be detected within Rhinocerotina, one including the South Asian taxa and *Lartetotherium* (node 2: 'Rhinoceroti' *sensu* Antoine *et al.* 2021: supported by seven unambiguous synapomorphies) and one including the African and Northern Eurasian species (node 3: 'Diceroti' *sensu* Antoine *et al.* 2021: supported by 14 unambiguous synapomorphies). Like in the topology obtained by Antoine *et al.* (2021), the relationships among the extant species support a geographic hypothesis rather than a horn hypothesis for the living rhinoceros species. The first dichotomy within the South Asian clade isolates the small clade (node 4) composed by *Lartetotherium* and *Gaindatherium*, as similarly obtained and discussed by several other analyses (Antoine *et al.* 2010; Pandolfi 2016). The second dichotomy (node 5) clusters the *Nesorhinus-Rhinoceros-Dicerorhinus* clade, composed by the extinct Philippine species *N. philippinensis*, the Sumatran rhinoceros (*D. sumatrensis*), the fossil Asian species from the Siwaliks,
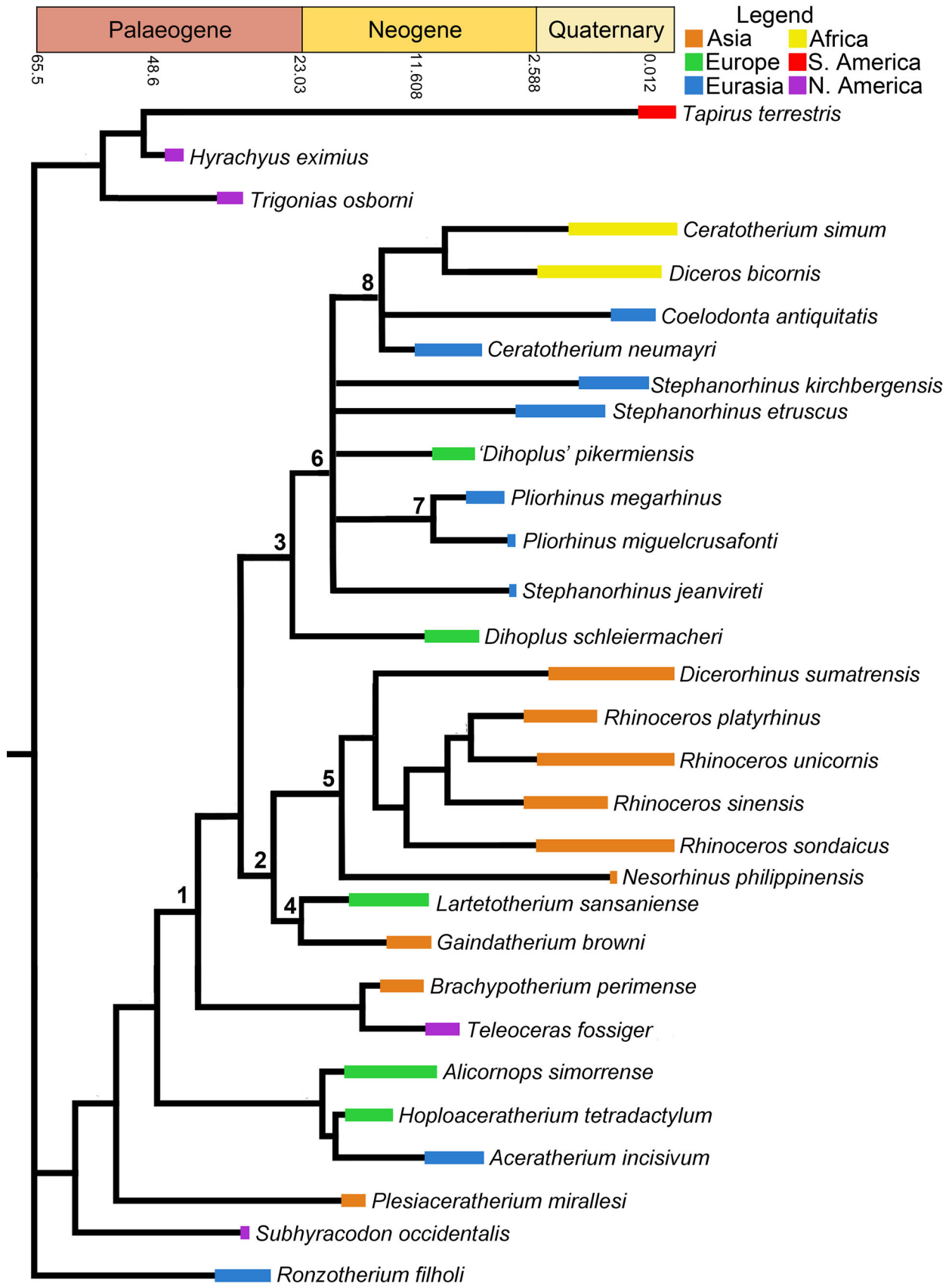
and the living one-horned rhinoceroses (*R. unicornis* and *R. sondaicus*) (Fig. 15). *Rhinoceros platyrhinus* is here retrieved as sister taxon to *R. unicornis*, as previously suggested by other scholars (Pandolfi & Maiorino 2016; Antoine *et al.* 2021). Within the African-Northern Eurasian clade, the first dichotomy isolated the Miocene *Dihoplus schleiermacheri*. A large polytomy is then present on the tree (node 6), concentrating all the discrepancies between the five most-parsimonious trees. Within this polytomy, a small clade composed by *P. miguelcrusafonti* and *P. megarhinus* (node 7) and a large one composed by the genera *Ceratotherium*, *Diceros* and *Coelodonta* (node 8) can be recognized (Fig. 15). The relationships of '*Dihoplus*' *pikermiensis*, *S. etruscus*, *S. jeanvireti* and *S. kirchbergensis* are not resolved here. The apomorphy list of the nodes in the consensus tree are reported in the Supplemental texts S3–S4.

The results obtained strongly support the clade composed by *P. miguelcrusafonti* and *P. megarhinus* here considered as coinciding with the new genus *Pliorhinus*. The clade is supported by 19 unambiguous synapomorphies (foramen infraorbitalis and nasal notch located above the molars, high zygomatic arch, occipital face backward inclined, developed nuchal tubercle, sub-triangular foramen magnum, P1 usually absent in adults, transverse metaloph on P2, protoloph always interrupted on P2, constriction of the protocone usually absent on P3 and P4, crista always present on P3, posterior part of the ectoloph concave on M1 and M2, constriction of the protocone always absent on M3, angular trigonid on the lower teeth, obtuse or right dihedron trigonid on the lower teeth, smooth anterior side of the semilunate, symmetric distal facet for the semilunar on the pyramidal, and curved magnum-facet on McII). *Pliorhinus* as a clade has the strongest Bremer support (Bremer index = 6) among Rhinocerotina (Supplemental text S4).

The type species of the new genus is *Pliorhinus megarhinus* (de Christol, 1834), diagnosed by 17 unambiguous synapomorphies (a flat dorsal profile of the skull, a convex processus postglenoidalis, labial cingulum usually absent on the upper premolars, crochet usually present on the upper premolars, protocone and hypocone forming a lingual bridge on the upper premolars, antecrochet usually absent on P4, labial cingulum usually absent on the upper molars, crista usually present on the upper molars, medifossette usually absent on the upper

molars, external groove vanishing before the neck on the lower teeth, lingual cingulum usually absent on the lower molars, ectolophid fold present on dp2 and dp3, anterodistal groove present on tibia, tibia and fibula independent, slender tuber calcanei, salient insertion of the m. fibularis longus on the calcaneus). *Pliorhinus miguelcrusafonti* is diagnosed by 11 unambiguous synapomorphies (a low base of the processus zygomaticus maxillari, a foramen mandibulare above teeth-neck level, a wrinkled aspect of the enamel, a multiple crochet on the premolars, a continuous or usually reduced lingual cingulum on the premolars, a wide postfossette on the premolars, no medifossette on P3 and P4, a constriction of the protocone usually present on P3, P4 and always present on M1 and M2, a posterior valley usually open on p2, secondary folds on DP2, trapezium-facet absent on McII).

The *Pliorhinus* clade is phylogenetically bracketed by *Dihoplus* and *Stephanorhinus* and the relationships within the latter genus are far from being solved, which is out of the scope of the current work.

Discussion

Pliorhinus miguelcrusafonti and its record
The rhinocerotine specimens from Kvabebi were partially published by Vekua (1972), who assigned them to *Dicerorhinus megarhinus*. Later, Tsiskarishvili (1987) erected the new species *Dicerorhinus vekuai* on the basis of a partial skull and mandible (GNM1 29-2013/925) and suggesting it has an evolved form of *D. megarhinus*. In any case, the Kvabebi rhinoceros displays the strongest similarities with the poorly known Pliocene rhinocerotine from Layna *Pliorhinus miguelcrusafonti* nov. comb. *Pliorhinus miguelcrusafonti* was described by Guérin & Santafé-Llopis (1978) on a fragment of mandible, isolated teeth (deciduous and a few permanent teeth) and some postcranial remains from Layna and a few specimens from Perpignan. *Pliorhinus miguelcrusafonti* was later recorded at La Calera (Teruel) by Cerdeño (1992) and at Alcalá del Júcar (Albacete) by Mazo (1997), based on a few isolated postcranial remains (Supplemental Table S1; Fig. 16). No other records of this taxon were recently reported in Eurasia.

Figure 15. Time-calibrated phylogeny of the taxa included in the cladistic analysis. The chronological ranges of the different species are after Guérin (1980), Heissig (1989, 1996, 1999), Cerdeño (1992), Prothero (2005), Pandolfi (2016), Pandolfi & Maiorino (2016), Pandolfi *et al.* (2015, 2016, 2017, 2019, 2020), Cirilli *et al.* (2020), Antoine *et al.* (2010, 2021). The consensus tree is obtained by PAUP 4.0β10 (Swofford 2001), heuristic search, TBR and 1000 replications with additional random sequence, gaps treated as missing (tree length = 1349 steps, consistency index = 0.274, retention index = 0.451, homoplasy index = 0.726). The data matrix is reported in Supplemental text S2.
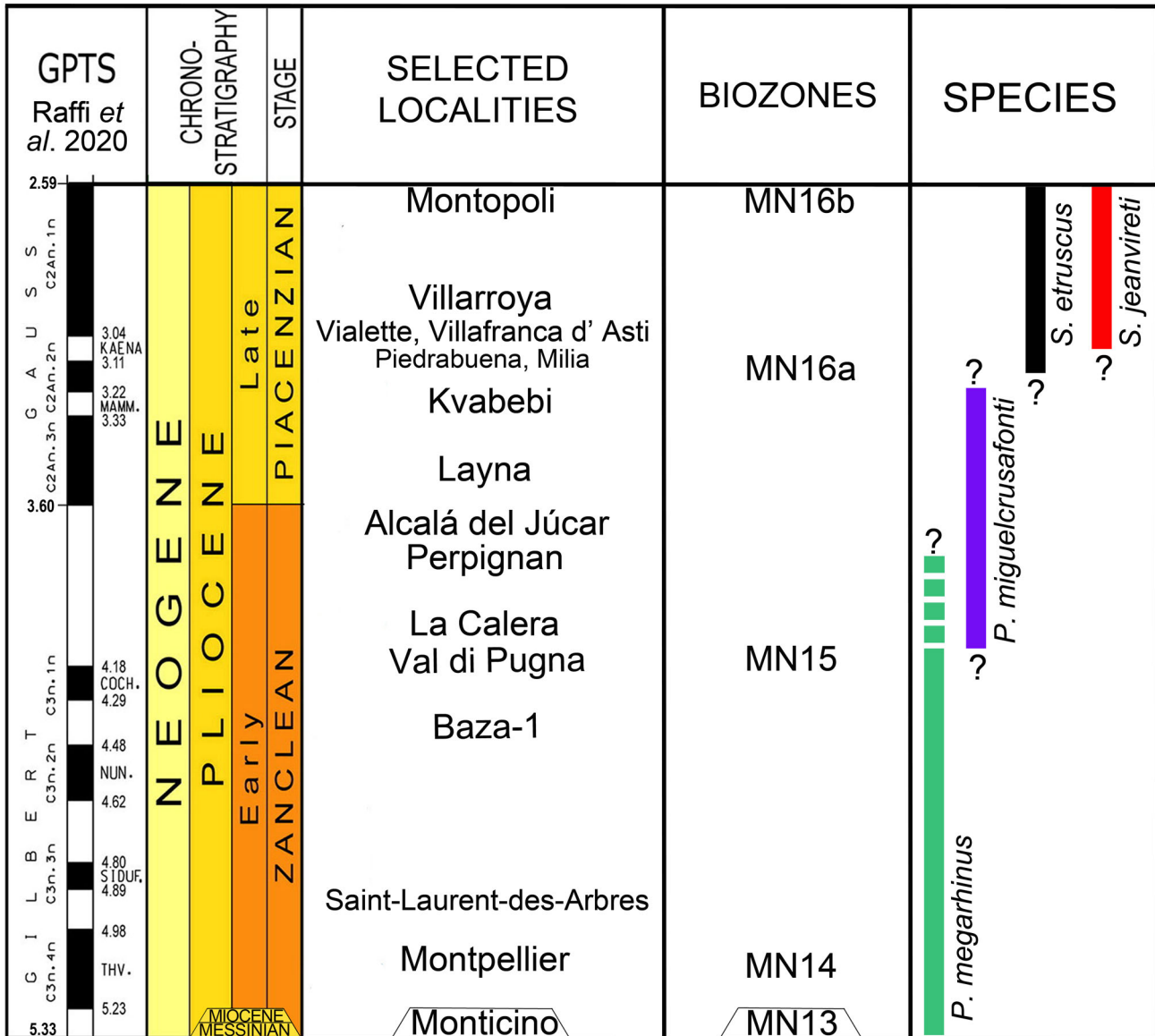
Figure 16. Chronostratigraphical correlations of the selected localities reported in Figure 1 and discussed in the text with the stratigraphic distribution of Pliocene and Early Pleistocene Western Eurasian rhinoceroses (chronostratigraphical scale after Raffi et al. 2020).

Our study of the specimens collected at Kvabebi provide here new insights into the morphological features and morphometric characters of this forgotten taxon, opening new perspectives in the evolutionary history and diversity of Pliocene rhinoceroses. For the first time, the associated cranial and postcranial remains allow us to recognize some diagnostic features of *P. miguelcrusafonti* and provide new considerations on its taxonomic position. A comparison with the type material from type areas of Northern Eurasian Pliocene species supported *P. miguelcrusafonti* as a valid taxon,

distinct from *P. megarhinus* and the *Stephanorhinus* species. A detailed comparison on postcranial remains provided useful key-characters to distinguish the studied species. However, as revealed by the morphological comparison, several characters are shared among the different species and only a combination of them would be useful to assign remains to a well-defined species; this would suggest a relatively wide uncertainty in the identification of fragmented or incomplete specimens. Likewise, the taxonomic assignment of isolated and worn-out teeth should be carefully evaluated. The specimens assigned to

P. miguelcrusafonti are somewhat dimensionally smaller than *P. megarhinus* and *S. jeanvireti* and sometimes are close to the largest specimens of *S. etruscus*.

The differences between *P. miguelcrusafonti* and *P. megarhinus* are based on dimension and morphology of the skull and postcranials. The morphological and morphometrical comparison between the considered specimens enabled us to assign some specimens from Perpignan, previously referred as *P. miguelcrusafonti* (namely the radius and the McII), to *P. megarhinus* thus confirming the sympatry of these two species during the Pliocene, as suggested by Guérin (1980). Sympatry within Rhinocerotidae, belonging or not to different genera, is commonly reported in literature and it is documented in the living African and Asian species (see Antoine 2012; Rookmaaker & Antoine 2013). Nevertheless, *Pliorhinus megarhinus* has not been unambiguously recorded in the Iberian Peninsula (Cerdeño 1992), and the unique record of this species, based on a proximal epiphysis of MtIV at Molins de Rei (Fernandez 2000), can be re-assigned to *P. miguelcrusafonti* due to the morphology of the bone.

A possible dispersal of *P. miguelcrusafonti* from Western Europe to the Caucasus seems to be suggested by the occurrences of this taxon; anyway, the records are still too scantly to reconstruct a valid pattern and, in the light of the new data here reported, several late Pliocene records of Europe need to be deeply revised. Numerous non-rhinocerotid elements of the Kvabebi fauna correspond to taxa of Eurasian affinities, such as *Hipparion roncinantis*, *Anancus arvernensis* and *Propotamochoerus provincialis*, that have been documented at Villafranca d'Asti (Triversa s.l.) in Italy, Les Etouaires in France, and Villarroya in Spain (MN16; Agustí *et al.* 2009). The occurrences of *Hipparion roncinantis*, *Vulpes alopecoides* and *Nyctereutes megamastoides* in the Kvabebi fauna (Rook *et al.* 2017; Cirilli *et al.* 2021) would suggest a dispersal from East to West of some taxa, predating their occurrence in Western Europe. Villarroya was claimed as one of the oldest localities that yielded remains of *S. etruscus* together with Piedrabuena and Las Higueruelas (Spain, latest Pliocene; Pandolfi *et al.* 2017; Supplemental Table S1; Fig. 16) whilst Villafranca d'Asti and Les Etouaires (Fig. 16) are characterized by the presence of *S. jeanvireti* (see discussion in Pandolfi *et al.* 2019) and a small-sized species usually referred to as *S. etruscus* (Cirilli *et al.* 2020) (Supplemental Table S1). The occurrence of *P. miguelcrusafonti* during the late Pliocene, from *c*. 4 Ma to 3 Ma (MN15-16a) and the similarities in size with *S. etruscus* would open new questions about the attribution of these relatively small-sized Western European remains normally assigned as *S. etruscus*.

Taxonomy and phylogeny

The cladistic analysis revealed that *P. miguelcrusafonti* is included within the Rhinocerotina clade and in particular that it is nested within Northern Eurasian and African Pliocene–Pleistocene rhinoceroses. More interestingly, it is sister species to *P. megarhinus* within the newly erected *Pliorhinus* genus.

Pliorhinus megarhinus and *P. miguelcrusafonti* have long suffered from a debated taxonomic position. They were frequently included into the genus *Dicerorhinus* (e.g. Guérin 1980, 1982), typified by the recent species *Dicerorhinus sumatrensis* (Fisher, 1814) (see Groves 1983; and the discussion in Pandolfi *et al.* 2015, 2016). Fortelius *et al.* (1993) referred the species *P. megarhinus* to *Stephanorhinus* and Cerdeño (1992, 1995) also included in this genus the species *P. miguelcrusafonti*. The latter taxon was dubitatively retained within *Stephanorhinus* by Pandolfi *et al.* (2015, 2016) due to the lack of well-preserved cranial remains useful to assess a generic assignment. The species *P. megarhinus* was also referred to the genus *Dihoplus* (e.g. Giaourtsakis 2003; Symeonidis *et al.* 2006; Lacombat & Mörs 2008) following the hypothesis proposed by Heissig (1989, 1996, 1999), who recognized an evolutionary lineage leading from the late Miocene *Dihoplus schleiermacheri* to *P. megarhinus* and another one ranging from *D. pikermiensis* to *S. etruscus*. The position of *P. megarhinus* within *Dihoplus* was never supported by strong evidence and the species was dubitatively retained within this genus only because of its dissimilarities with *Stephanorhinus* (Pandolfi *et al.* 2015, 2016, 2019, 2020).

Distinct lineages, originated from a common Miocene ancestor, are here recognized (Fig. 15). The clade formed by *P. miguelcrusafonti* and *P. megarhinus*, here referred to the new genus *Pliorhinus*, represents a distinct late Neogene lineage in respect to *Stephanorhinus*. The latter genus results as paraphyletic, as recently evidenced by Cappellini *et al.* (2019) and Antoine *et al.* (2021). The study of the phylogenetic relationships within *Stephanorhinus* and the discussion about its paraphyly are beyond the aims of this work. Recent phylogenomic analyses (Liu *et al.* 2021) also highlighted contrasting results obtained by means of morpho-anatomical, mitogenomic and palaeoproteomic approaches, providing support for the geographical hypothesis of rhinoceros evolution (Liu *et al.* 2021) rather than for a horn-hypothesis (Cappellini *et al.* 2019). In this framework, three major clades have been detected, one composed by the two extant African species *C. simum* and *D. bicornis*, one composed by the Sumatran (*D. sumatrensis*), the Merck's (*S. kirchbergensis*) and the woolly (*C. antiquitatis*) rhinoceroses, and a third one which includes the *Rhinoceros* species; the latter two clades are more closely related to each other than to the

African lineage (Liu *et al.* 2021). However, understanding the relationships among the extinct Eurasian rhinoceroses, without DNA preservation, still remains a challenge in phylogenetic studies.

Conclusions

Pliocene rhinoceroses are poorly documented in Eurasia and still far to be well understood from phylogenetic, taxonomic, and historical biogeographical perspectives. Fossil specimens from early Pliocene times were usually assigned to *Stephanorhinus megarhinus* and those from the latest Pliocene to *Stephanorhinus jeanvireti*. The species *Dicerorhinus miguelcrusafonti* erected by Guérin & Santafé-Llopis (1978) was only reported in a few localities of Western Europe (Layna, La Calera, Alcalá del Júcar and Perpignan) thus far and it has accordingly been regarded as an endemic Western European taxon, ambiguously assigned to the genus *Stephanorhinus*. Skulls and complete mandibles were unknown before this work and the systematic position of the species, only based on a few postcranials, appeared to be problematic. The new data from Kvabebi, Georgia, add new knowledge on this forgotten rhinocerotine, suggesting a close relationship with '*Stephanorhinus*' *megarhinus* within the new genus *Pliorhinus*. In addition, the material from Kvabebi contributes in clarifying its taxonomic position, and opens a new perspective in the phylogenetic relationships of Pliocene–Pleistocene rhinoceroses of Eurasia. A deep morphological comparison allows us to depict a clearer framework on the morphological differences among the considered Pliocene species, providing additional and more complete information on cranial and postcranial remains of *Pliorhinus miguelcrusafonti*. Finally, the cladistic analysis here performed, useful to clarify the affinity of the rhinoceros from Kvabebi, represents a starting point towards a better understanding of the Northern Eurasian post-Miocene Rhinocerotidae and their phylogenetic relationships.

Acknowledgements

Supplemental material

Supplemental material for this article can be accessed here: http://dx.doi.org/10.1080/14772019.2021.1995907. A list of files can be found in Supplemental material S1.

ORCID

Luca Pandolfi http://orcid.org/0000-0002-4186-4126
Antoine Pierre-Olivier http://orcid.org/0000-0001-9122-1818
Maia Bukhsianidze http://orcid.org/0000-0002-6505-7097
David Lordkipanidze http://orcid.org/0000-0003-4894-4038
Lorenzo Rook http://orcid.org/0000-0001-8923-5428

References

Agustí, J., Vekua, A., Oms, O., Lordkipanidze, D., Bukhsianidze, M., Kiladze, G. & **Rook, L.** 2009. The Pliocene–Pleistocene succession of Kvabebi (Georgia) and the background to the early human occupation of Southern Caucasus. *Quaternary Science Reviews*, **28**, 3275–3280.

Antoine, P.-O. 2002. Phylogénie et évolution des Elasmotheriina (Mammalia, Rhinocerotidae). *Mémoires du Muséum national d'Histoire naturelle*, **188**, 1–359.

Antoine, P.-O. 2012. Pleistocene and Holocene rhinocerotids (Mammalia, Perissodactyla) from the Indochinese Peninsula. *Comptes Rendus Palevol*, **11**, 159–168.

Antoine, P.-O., **Downing, K. F.**, **Crochet, J. Y.**, **Duranthon, F.**, **Flynn, L. J.**, **Marivaux, L.**, **Métais, G.**, **Rajpar, A. R.** & **Roohi, G.** 2010. A revision of *Aceratherium blanfordi* Lydekker, 1884 (Mammalia: Rhinocerotidae) from the Early Miocene of Pakistan: postcranials as a key. *Zoological Journal of the Linnean Society*, **160**, 139–194.

Antoine, P.-O., **Reyes, M. C.**, **Amano, N.**, **Claude, J.**, **Bautista, A.P.**, **Vos, J. de** & **Ingicco, T.** 2021. A new clade of rhinoceroses from the Pleistocene of Southeast Asia sheds light on mainland mammal dispersals to the Philippines. *Zoological Journal of the Linnean Society*. doi:10.1093/zoolinnean/zlab009

Bukhsianidze, M. & **Koiava, K.** 2018. Synopsis of the terrestrial vertebrate faunas from the Middle Kura Basin (Eastern Georgia and Western Azerbaijan, South Caucasus). *Acta Palaeontologica Polonica*, **63**(3), 441–461.

Cappellini, E., **Welker, F.**, **Pandolfi, L.**, **Ramos-Madrigal, J.**, **Samodova, D.**, **Rüther, P. L.**, **Fotakis, A. K.**, **Lyon, D.**, **Moreno-Mayar, J. V.**, **Bukhsianidze, M.**, **Jersie-Christensen, R. R.**, **Mackie, M.**, **Ginolhac, A.**, **Ferring, R.**, **Tappen, M.**, **Palkopoulou, E.**, **Dickinson, M. R.**, **Stafford, T. W. Jr**, **Chan, Y. L.**, **Götherström, A.**, **Nathan Senthilvel, K. S. S.**, **Heintzman, P. D.**, **Kapp, J. D.**, **Kirillova, I.**, **Moodley, Y.**, **Agustí, J.**, **Kahlke, R.-D.**, **Kiladze, G.**, **Martínez-Navarro, B.**, **Liu, S.**, **Velasco, M. S.**, **Sinding, M.-H. S.**, **Kelstrup, C. D.**, **Allentoft, M. E.**, **Orlando, L.**, **Penkman, K.**, **Shapiro, B.**, **Rook, L.**, **Dalén, L.**, **Gilbert, M. T. P.**, **Olsen, J. V.**, **Lordkipanidze, D.** & **Willerslev, E.** 2019. Early Pleistocene enamel proteome from Dmanisi resolves *Stephanorhinus* phylogeny. *Nature*, **574**, 103–107.

Cerdeño, E. 1992. Spanish Neogene rhinoceroses. *Paleontology*, **35**, 297–308.

Cerdeño, E. 1995. Cladistic analysis of the family Rhinocerotidae (Perissodactyla). *American Museum Novitates*, **3143**, 1–25.

Cirilli, O., **Pandolfi, L.** & **Bernor, R. L.** 2020. The Villafranchian Perissodactyls of Italy: the knowledge of the fossil record and future research perspectives. *Geobios*, **63**, 1–21.

Cirilli, O., **Bernor, R. L.** & **Rook, L.** 2021. New insights on the Early Pleistocene equids from Roca-Neyra (France, central Europe): implications for the *Hipparion* LAD and the *Equus* FAD in Europe. *Journal of Paleontology*, **95**(2), 406–425.

Cuvier, G. 1822. *Recherches sur les ossemens fossiles de quadrupedes, nouvelle édition*, Volume 2. G. Dufour et E. D'Ocagne, Paris, 684 pp.

de Christol, J. 1834. Recherches sur les caractères des grandes espèces de Rhinocéros fossiles. *Annales des Sciences Naturelles, Paris, series 2*, **4**, 44–112.

Falconer, H. 1868. On the European Pliocene and Post-Pliocene species of the genus *Rhinoceros*. Pp. 309–403 in C. Murchison (ed.) *Palaeontological memoirs and notes of the late Hugh Falconer, (2) mastodon, elephant, rhinoceros, ossiferous caves, primeval man and his contemporaries*. Charles Murchison, Robert Hardwicke, London.

Fernandez, D. G. 2000. *Stephanorhinus megarhinus* (Rhinocerotidae) en el Plioceno de Molins De Rei, Baix Llobregat (Barcelona). *Butlletí del Centre d'Estudis de la Natura del Barcelonas-Nord*, **5**(1), 47–51.

Fischer, G. 1814. *Zoognosia: tabulis synopticis illustrate*. N. S. Vsevolozsky, Moscow, 732 pp.

Fortelius, M., **Mazza, P.** & **Sala, B.** 1993. *Stephanorhinus* (Mammalia: Rhinocerotidae) of the Western European Pleistocene, with a revision of *S. etruscus*, Falconer, 1868. *Palaeontographia Italica*, **80**, 63–155.

Giaourtsakis, I. X. 2003. *Late Neogene Rhinocerotidae of Greece: distribution, diversity and stratigraphical range*. *Deinsea*, **10**, 235–253.

Gray, J. E. 1821. On the natural arrangement of vertebrose animals. *London Medical Repository*, **15**, 296–310.

Groves, C. P. 1983. Phylogeny of the living species of rhinoceros. Zeitschriften für Zoologische *Systematik und Evolutionsforschung*, **21**, 293–313.

Guérin, C. 1972. Une nouvelle espèce de Rhinocéros (Mammalia, Perissodactyla) à Vialette (Haute-Loire, France) et dans d'autres gisements du Villafranchien Inférieur Européen: *Dicerorhinus jeanvireti* n. sp. *Documents des Laboratoires de Géologie de la Facultè des Sciences de Lyon*, **49**, 53–161.

Guérin, C. 1980. Les rhinoceros (Mammalia, Perissodactyla) du Miocene terminal au Pleistocene superieur en Europe occidentale; comparaison avec les especes actuelles. *Documents du Laboratoire de Geologie de la Faculte des Sciences de Lyon*, **79**, 3–1183.

Guérin, C. 1982. Première biozonation du Pléistocène européen, principal résultat biostratigraphique de l'étude des Rhinocerotidae (Mammalia, Perissodactyla) du Miocène terminal au Pléistocène supérieur d'Europe occidentale. *Geobios*, **15**, 593–598.

Guérin, C., **Ballesio, R.** & **Méon-Villain, H.** 1969. Le *Dicerorhinus megarhinus* (Mammalia, Rhinocerotidae) du Pliocène de Saint-Laurent-des-Arbres (Gard). *Documents des Laboratoires de Géologie de Lyon*, **31**, 55–145.

Guérin, C. & **Santafé-Llopis, J. V.** 1978. *Dicerorhinus miguelcrusafonti* nov. sp., une nouvelle espèce de rhinocéros (Mammalia, Perissodactyla) du gisement Pliocène supérieur de Layna (Soria, Espagne) et de la formation Pliocène de Perpignan (Pyrénées-Orientales, France). *Geobios*, **11**(4), 457–491.

Guérin, C. & **Tsoukala, E.** 2013. The Tapiridae, Rhinocerotidae and Suidae (Mammalia) of the Early Villafranchian site of Milia (Grevena, Macedonia, Greece). *Geodiversitas*, **35**(2), 447–489.

Heissig, K. 1989. The Rhinocerotidae. Pp. 399–417 in D. R. Prothero & R. M. Schoch (eds) *The evolution of Perissodactyls*. Oxford Monographs on Geology and Geophysics, Volume 15, New York.

Heissig, K. 1996. The stratigraphical range of fossil rhinoceroses in the Late Neogene of Europe and Eastern Mediterranean. Pp. 339–347 in R. L. Bernor, V. Fahlbush, & H.-W. Mittman (eds) *The evolution of Western Eurasian Neogene mammal faunas*. Columbia University Press, New York.

Heissig, K. 1999. Family Rhinocerotidae. Pp. 175–188 in G. E. Rössner, & K. Heissig (eds) *The Miocene land mammals of Europe*, Pfeil, Munich.

Lacombat, F. & **Mörs, T.** 2008. The northernmost occurrence of the rare Late Pliocene rhinoceros *Stephanorhinus jeanvireti* (Mammalia, Perissodactyla). *Neues Jahrbuch für Geologie und Paläontologie*, *Abhandlungen*, **249**(2), 157–165.

Lazarev, S. 2020. *From the Eastern Paratethys to the Pontocaspian basins: late Miocene–Middle Pleistocene magneto-biostratigraphy, sedimentary architecture and faunal turnovers of the shrinking basins of West Eurasia.* PhD dissertation, Utrecht University, doi:10.33540/51

Liu, S., **Westbury, M. V.**, **Dussex, N.**, **Mitchell, K. J.**, **Sinding, M.-H. S.**, **Heintzman, P. D.**, **Duchêne, D. A.**, **Kapp, J. D.**, **von Seth, J.**, **Heiniger, H.**, **Sánchez-Barreiro, F.**, **Margaryan, A.**, **André-Olsen, R.**, **De Cahsan, B.**, **Meng, G.**, **Yang, C.**, **Chen, L.**, **van der Valk, T.**, **Moodley, Y.**, **Rookmaaker, K.**, **Bruford, M. W.**, **Ryder, O.**, **Steiner, C.**, **Bruins-van Sonsbeek, L. G. R.**, **Vartanyan, S.**, **Guo, C.**, **Cooper, A.**, **Kosintsev, P.**, **Kirillova, I.**, **Lister, A. M.**, **Marques-Bonet, T.**, **Gopalakrishnan, S.**, **Dunn, R. R.**, **Lorenzen, E. D.**, **Shapiro, B.**, **Zhang, G.**, **Antoine P.-O.**, **Dalén, L.** & **Gilbert, M. T. P.** 2021. Ancient and modern genomes unravel the evolutionary history of the rhinoceros family. *Cell*, **184**, 1–12.

Mazo, A. V. 1997. El yacimiento rusciniense de Alcalá del Júcar (Albacete). Taxonomía y Biostratigrafía. *Estudios Geológicos*, **53**(5–6), 275–286.

Owen, R. M. 1848. Description of teeth and proportion of jaws of two extinct anthracotherioid quadrupeds (*Hyopotamus vectianus and Hyopotamus bovinus*) discovered by the Marchioness of Hastings in the Eocene deposits on the NW coast of the Isle of Wight: with an attempt to develop Cuvier's idea of the classification of pachyderms by the number of their toes. *Quarterly Journal of the Geological Society of London*, **4**, 103–141.

Pandolfi, L. 2016. *Persiatherium rodleri*, gen. et sp. nov. (Mammalia, Rhinocerotidae), from the Late Miocene of Maragheh (Northwestern Iran). *Journal of Vertebrate Paleontology*, **36**, e1040118, 1–8.

Pandolfi, L., **Gasparik, M.** & **Piras, P.** 2015. Earliest occurrence of *"Dihoplus" megarhinus* (Mammalia, Rhinocerotidae) in Europe (Late Miocene, Pannonian Basin, Hungary): Palaeobiogeographical and biochronological implications. *Annales de Paléontologie*, **101**(4), 325–339.

Pandolfi, L. & **Maiorino, L.** 2016. Reassessment of the largest Pleistocene rhinocerotine *Rhinoceros platyrhinus* (Mammalia, Rhinocerotidae) from the Upper Siwaliks (Siwalik Hills, India). *Journal of Vertebrate Paleontology*, **36**(2), 1_12, e1071266.

Pandolfi, L., **Gasparik, M.** & **Magyar, I.** 2016. Rhinocerotidae from the upper Miocene deposits of the Pannonian Basin (Hungary): implications for migration routes and biogeography. *Geologica Carpathica*, **67**(1), 69–82.

Pandolfi, L., **Cerdeño, E.**, **Codrea, V.** & **Kotsakis, T.** 2017. Biogeography and chronology of the Eurasian extinct rhinoceros *Stephanorhinus etruscus*, Mammalia, Rhinocerotidae. *Comptes Rendus Palevol*, **16**(7), 762–773.

Pandolfi, L., **Popescu, A.** & **Codrea, V.** 2019. *Stephanorhinus jeanvireti* (Mammalia, Rhinocerotidae) from the early Pleistocene of Colţeşti, southwestern Romania. *Comptes Rendus Palevol*, **18**(8), 1041–1056.

Pandolfi, L., **Rivals, F.** & **Rabinovich, R.** 2020. A new species of rhinoceros from the site of Bethlehem: "*Dihoplus*" *bethlehemsis* sp. nov. (Mammalia, Rhinocerotidae). *Quaternary International*, **537**, 48–60.

Prothero, D. R. 2005. *The evolution of North American rhinoceroses*. Cambridge University Press, New York, 218 pp.

Raffi, I., **Wade, B. S.**, **Pälike, H.**, **Beu, A. G.**, **Cooper, R.**, **Crundwell, M. P.**, **Krijgsman, W.**, **Moore, T.**, **Raine, I.**, **Sardella, R.** & **Vernyhorova, Y. V.** 2020. The Neogene Period. Chapter 29. Pp. 1141–1215 in F. M. Gradstein, J. G. Ogg, M. D. Schmitz & G. M. Ogg (eds) *Geologic time scale 2020*. Elsevier, Amsterdam.

Rook, L., **Bartolini Lucenti, S.**, **Bukhsianidze, M.** & **Lordkipanidze, D.** 2017. The Kvabebi Canidae record revisited (late Pliocene, Sighnaghi, eastern Georgia). *Journal of Paleontology*, **91**(6), 1258–1271.

Rookmaaker, L. C. & **Antoine, P.-O.** 2013. New maps representing the historical distribution of the African species of rhinoceros: *Diceros bicornis*, *Ceratotherium simum* and *Ceratotherium cottoni*. *Pachyderm*, **52**, 91–96.

Swofford, D. L. 2001. *PAUP* (phylogenetic analysis using parsimony [*and other methods] version 4.0β10)*. Sinauer, Sunderland, MA.

Symeonidis, N. K., **Giaourtsakis, I. X.**, **Seeman, R.** & **Giannopoulos, V. I.** 2006. Aivaliki, a new locality with fossil Rhinoceroses near Alistrati (Serres, Greece). *Beiträge zur Paläontologie*, **30**, 437–451.

Tsiskarishvili, G. V. [**Tsiskarišvili, G. V.**] 1987. Pozdnetretičnye Nosorogi (Rhinocerotidae) Kavkaza. Mecniereba, Tbilisi, 142 pp. [In Russian.]

Vekua, A. 1972. [*Kvabebi Fauna of Akchagylian Vertebrates*]. Moscow, Nauka, 258 pp. [In Russian.]

Vekua, A. & **Lordkipanidze, D.** 2008. The history of vertebrate fauna in Eastern Georgia. *Bulletin of the Georgian National Academy of Science*, **2**(3), 149–155.

Associate Editor: Adrian Lister